Chapter 6. RESULTS

This chapter analyzes monthly and annual performance estimates made with the new simplified direct-coupled PV model (DCPVSIMP) in three ways. In Sections 6.1 and 6.2 different statistical evaluations of the DCPVSIMP model's results are compared to other performance models. In Section 6.3 a series of illustrations showing applications of the DCPVSIMP model for direct-coupled PV system design are analyzed.

A summary of the interpretations and conclusions from Sections 6.1 - 6.3 is provided in Section 6.4, and recommendations for in1provements and continued study are given in Section 6.5.

The primary use of the DCPVSIMP model is for predicting the long-term output of direct-coupled, in addition to maximum power-tracked, PV systems. No simple and comprehensive means of assessing the accuracy of this model are available. As explained in Sections 2.2 and 5.3, alternative models which have been validated elsewhere, such as PV f-Chart and PVFORM [21,22], are limited to maximum power-tracked systems. However, as an initial screening measure, the performance of the DCPVSIMP model and the new detailed direct-coupled PV model (DCPVDET) for maximum power-tracked systems may be compared to like cases modeled with PV f-Chart and PVFORM. This comparison is made in Section 6.1.

Satisfactory predictions of maximum power-tracked performance are a minimum requirement for a direct-coupled performance model. Additional comparisons are needed

to evaluate the accuracy of the DCPVSIMP model for direct-coupled system performance. To accomplish this, a wide range of simulations comparing the DCPVSIMP and DCPVDET models have been devised. The various factors/values which were used to create the range of simulations were described in Section 5.3. The results are presented in Section 6.2.

There are several reasons why the DCPVDET model has been accepted here as an appropriate reference for evaluating the DCPVSIMP model. One reason, as will be shown in the results of the following section, is that the DCPVDET model is in excellent agreement with predicted long-term maximum power-tracked performance using the PV i-Chart and PVFORM models. This result is as expected; the I-V curve component of the DCPVDET model is the UP I-V curve model, which was shown in Section 2.8.2- to agree well with experimental maximum power-point data and also with the linear model used in PV f-Chart and PVFORM.

Another reason is that the DCPVDET model uses actual hour by hour weather data. As a result, it does not rely on weather data correlations (described in Chapter 4) as does the DCPVSIMP model

The sources of uncertainty in the DCPVDET and DCPVSIMP models are the array and load I-V curve sub-models. (The DCPVSIMP and DCPVDET models both use the same array and load I-V curve sub-models.) The array I-V curve sub-model was evaluated in Section 2.8.1 and shown to match well with experimental I-V curves

measured under a wide variety of conditions. The DCPVDET and DCPVSIMP models integrate the power from a series of I-V curves each timestep. The load I-V curve sub-model is better determined than the array I-V curve sub-model because the load I-V curve is either (a) known from measured data, (b) given as a fixed voltage, or (c) given as a fixed resistance which obeys Ohm's Law. Solving for the hourly operating point and then integrating the results over monthly and annual periods are both analytical, straightforward, and precise operations that are not believed to be significant sources of error. Therefore, it is assumed that the DCPVDET model properly simulates direct-coupled system performance, as it uses measured load and weather data and an array sub-model of proven accuracy.

In Section 6.3, the DCPVSIMP model results are analyzed is by applying the model to some typical designs and developing sensitivity curves. The predicted sensitivity to any variety of design factors (e.g., module, motor, or pump type, or the number of series and parallel modules in the array) can be used to optimize direct-coupled system designs.

6.1 Predicted Maximum Power- Tracked Performance Comparison

To assess whether the DCPVSIMP and DCPVDET models are consistent with two established models, PV i-Chart and PVFORM, 12 cases were run with each of the four models. A 5 "typical day" segment approximation was used for the DCPVSIMP model. The 12 cases included 2 fixed array tilt angles (tilt = latitude, tilt = horizontal) at each of 6 locations (Albuquerque, Madison, Seattle, New York city, Nashville, and Miami). These locations were selected to provide a wide range of climatic conditions

ranging from uniformly clear (Albuquerque) to uniformly hazy (Miami), and from wide seasonal variations (Seattle, Madison) to moderate seasonal variations (New York, Nashville). Three results from each case are used in this evaluation: January, July, and annual predicted maximum power-tracked DC electric output.

The same array was modeled for each case (based on an actual 47.3 m^2, ≈4500 W Tri-Solar Corp. array at the Southwest Regional Experiment Station in Las Cruces. NM), and identical assumptions were used throughout for items such as the maximum power-tracker and power conditioning unit efficiencies (100%), ground reflectance (0.2), temperature coefficient of maximum power (0.004/ºC), and array reference power characteristics (cell temperature of 48 °C at 1018 W/m^2 irradiance, maximum power current of 26 A at 179 V, short circuit current of 29 A and open circuit voltage of 227 V).

Figure 54 shows how the four models compare over all 12 cases. The results have been normalized so that the total output for each model over each period is expressed relative to that predicted by the DCPVDET model. Except for the PV f-Chart model, the differences between models are insignificant. The PV f-Chart model is generally about 5% lower than the others. This difference is likely due to the fact that PV f-Chan automatically adjusts (decreases) the cover transmittance-absorptance product at non-normal incidence angles [56]. The other models do not consider this factor.

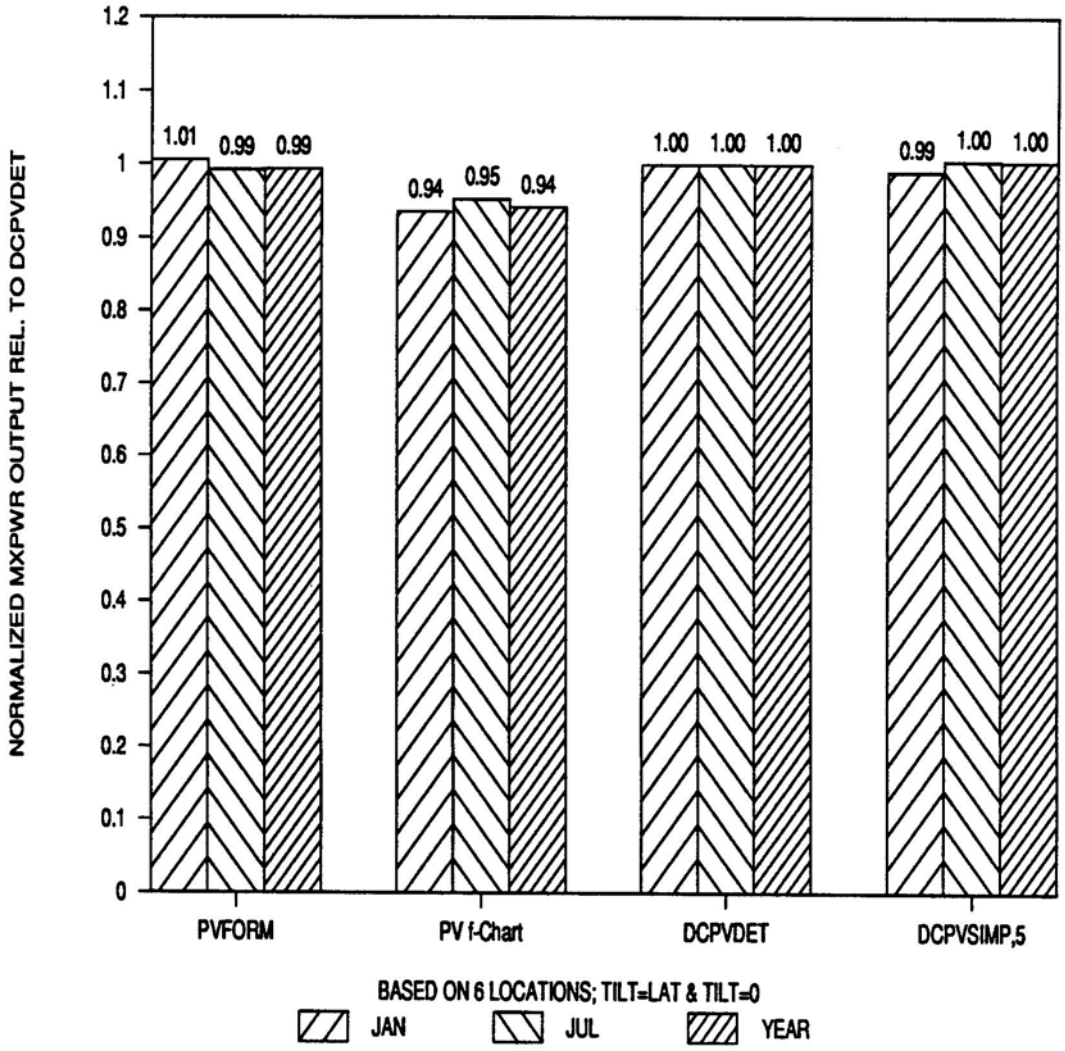

Figure 54. Relative Predicted Maximum Power-Tracked Output for 4 models

Figure 55 and 56 show how the models compare when the horizontal and tilted cases are isolated. The tilt = latitude cases are more important for most designs, as this angle maximizes (approximately) overall annual output. For most northern latitudes, the horizontal cases increase summer output but greatly decrease winter output. The differences between the DCPVSIMP and DCPVDET models are insignificant. The

differences between these and the PV f-Chart model are similar to those shown in Figure 54, except for January, where the horizontal surface predicted output is about 13% less than that predicted by the DCPVDET model. This result is an extreme example of how the incidence angle modifier affects the calculations for absorbed energy; for this orientation and time of year, the incidence angle is always large for northern latitudes. The other notable result is that the PVFORM model output is more sensitive to the tilt angle, especially in January, with relatively greater output at the moderate tilt and lower output at zero tilt. This behavior results because the PVFORM model uses the Perez anisotropic sky model for calculating diffuse radiation, while the other models assume an isotropic sky. Reindl [57] notes a similar trend in his comparison of anisotropic sky models relative to the isotropic sky model.

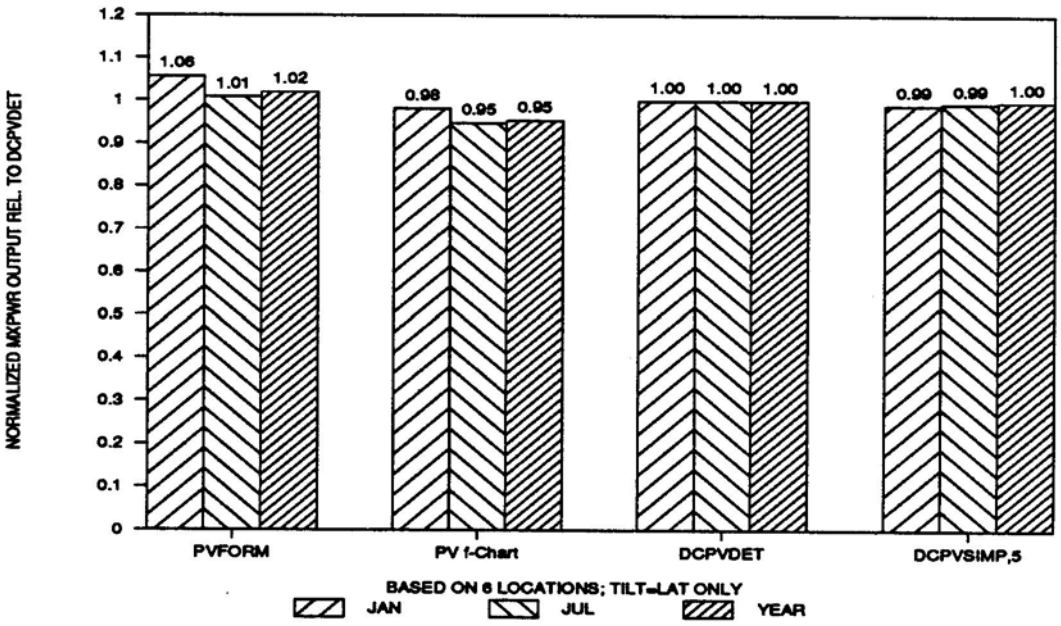

Figure 55. Relative Output for 4 Models, Tilt = Lat.

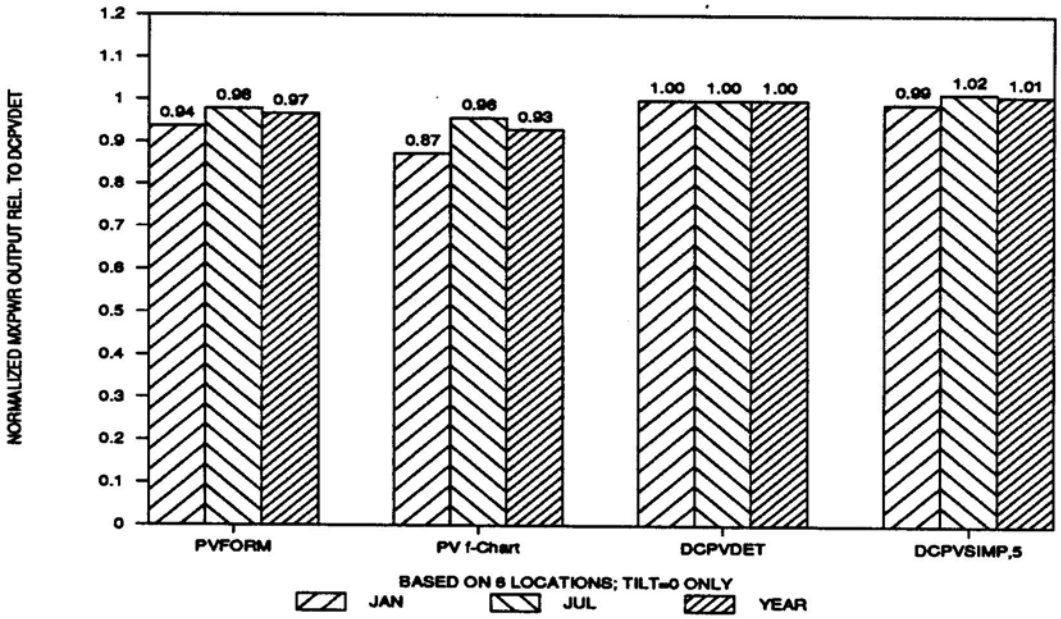

Figure 56. Relative Output for 4 Models, Tilt = Horiz.

Figure 57 shows how the annual kWh output of four models compare at each location, at a tilt angle equal to the latitude. The predicted DCPVSIMP model output is nearly identical to that predicted by the DCPVDET model for each city, is always within ± 5% of the other two models, and generally falls between them.

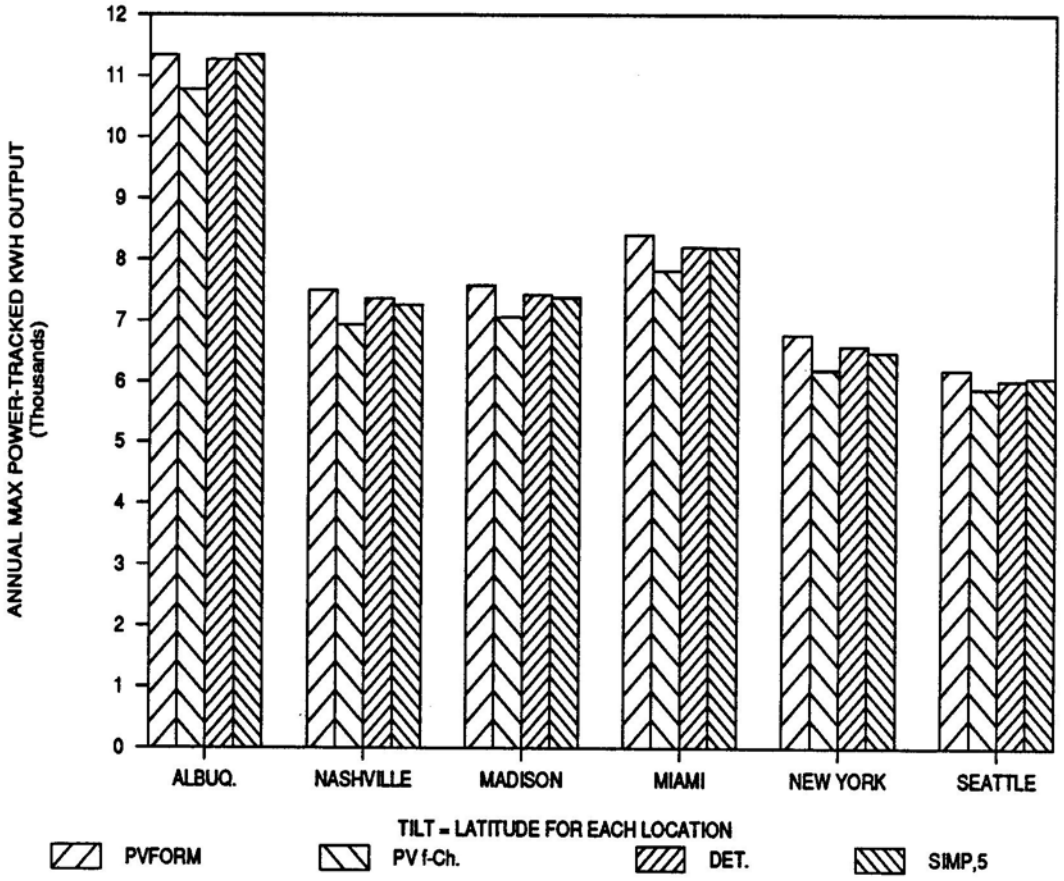

Figure 57. Annual Output by Location, Tilt = Lat.

Appendix E includes additional graphs showing the predicted annual kWh output at each location for a horizontal array, and the January and July output for both tilt = latitude and horizontal cases. Table E-l in Appendix E lists the raw output data for each month, each case, and each model.

The overall conclusion from this maximum power-tracked model comparison is that the DCPVDET model and the 5 segment DCPVSIMP model are consistent with two established models, PV f-Chan and PVFORM, and that these new models adequately predict maximum power-tracked system output over a typical range of U.S. climates, and over any monthly or annual period.

6.2 Simulation Results: DCPVSIMP vs. DCPVDET models

This section presents comparisons between four versions of the DCPVSIMP model and the DCPVDET model. Comparisons for annual, January, and July output are included, based on 816 different direct-coupled system configurations, or cases, as described in Section 5.3. The cases have been devised to simulate a broad range of climates, module/array types and sizes, and applied loads. The intent of the comparisons is to determine whether any version of the DCPVSIMP model can satisfactorily predict long-term direct-coupled system behavior, and to identify which factors are important influences on the model's accuracy.

Throughout the following analyses, all statistics for the simplified model will be calculated relative to the detailed model, either as an absolute root mean square

difference (RMS) in units of kWh using Eqn. 6.3, as a dimensionless % RMS using Eqn. 6.4, or as a dimensionless % mean bias difference (MBD) using Eqn. 6.5. The dimensionless % RMS and % MBD quantities are normalized relative to the detailed model's weighted-average kWh output for the cases of interest. The detailed model weighted-average kWh, $\overline{kWh}_{DET}$, is defined as the point where the sum of the moments, $\sum M_i$, of "N" cases, equals zero:

$$0 = \sum_{}^{N} M_i = \sum_{}^{N} kWh_{DET,i}(\overline{kWh}_{DET} - kWh_{DET,i}) \tag{6.1}$$

Rearranging to solve for $\overline{kWh}_{DET}$,

$$\overline{kWh}_{DET} = \frac{\sum\left(kWh_{DET,i}^2\right)}{\sum kWh_{DET,i}} \tag{6.2}$$

$$RMS \quad DIFF. = \left[\frac{\sum\left(kWh_{SIMP.} - kWh_{DET.}\right)^2}{N}\right]^{1/2} \tag{6.3}$$

$$\%RMS \quad DIFF. = \left[\frac{\sum\left(kWh_{SIMP.} - kWh_{DET.}\right)^2}{N}\right]^{1/2} \cdot \frac{100}{\overline{kWh}_{DET}} \tag{6.4}$$

$$\%MBD \quad DIFF. = \left[\frac{\sum\left(kWh_{SIMP.} - kWh_{DET.}\right)}{N}\right] \cdot \frac{100}{\overline{kWh}_{DET}} \tag{6.5}$$

6.2.1 Annual Results

Table 13 summarizes the relative differences between the annual direct-coupled output predicted by four versions of the DCPVSIMP model (3, 5, 10, and 20 "typical day" segments) and the DCPVDET model over all 816 cases, that is, over every

combination of location, module/array, and load described in Section 5.3. These results are also broken down by location, using 272 cases (1/3 of 816) for each city.

A general trend evident in this table is that both the mean bias and RMS statistics improve when the number of segments is increased due to the greater accuracy of the monthly Kr curve approximation. Most of the improvement occurs when the segments are increased from three to five, with a diminishing improvement beyond five segments. This trend is illustrated by Figure 58.

Table 13. DCPVSIMP vs. DCPVDET: % RMS and % MBD, Annual Summary

DCPVSIMP # segs. =>	3	5	10	20
All cases, % MBD	0.7	0.5	0.4	0.4
All cases, % RMS	3.8	3.4	3.3	3.2
All cases, RMS kWh	182	165	159	155
All cases, % MBD for max power-tracking	0.3	0.1	0.0	-0.1
All cases, % RMS for max power-tracking	0.7	0.4	0.4	0.4
Albuq. % MBD	1.1	0.9	0.7	0.6
Albuq. % RMS	3.7	3.4	3.2	3.1
Mad. % MBD	0.2	0.0	0.0	-0.1
Mad. % RMS	4.4	3.9	3.8	3.8
Sea. % MBD	0.5	0.6	0.7	0.7
Sea. % RMS	4.1	3.7	3.6	3.5

An exception to the trend of improved accuracy with an increase in number of segments is the % MBD for Seattle, which slowly increases with the number of segments, even though the % RMS decreases. The primary difference with the Seattle climate is that for five months of the year, the general shape of the Kr distribution curve is concave up (refer to Sections 4.2, 4.3); this is true for just one month in Madison and none in

Albuquerque. When the concave up shape occurs, increasing the number of segments increases the estimated radiation (if all segments are of equal width and their height is determined based on the midpoint of each segment). With an increase in estimated radiation, there is a corresponding increase in estimated power output and consequently, an increase in the % MBD relative to the TMY-based detailed model.

Figure 59 is a plot of the predicted annual kWh output from the DCPVSIMP model (points for 3 and 20 segment versions are shown) versus the predicted kWh output from the DCPVDET model for 816 cases. The figure shows a good correspondence between both versions of the DCPVSIMP model and the DCPVDET model, with data scattered fairly evenly on each side of the "perfect fit" line. The figure also shows a smaller spread of data points with the 20 segment version, consistent with the smaller RMS difference calculated for the 20 segment version than for the 3 segment version. Possible causes of the scatter seen in this plot will be examined in detail in the remainder of this section.

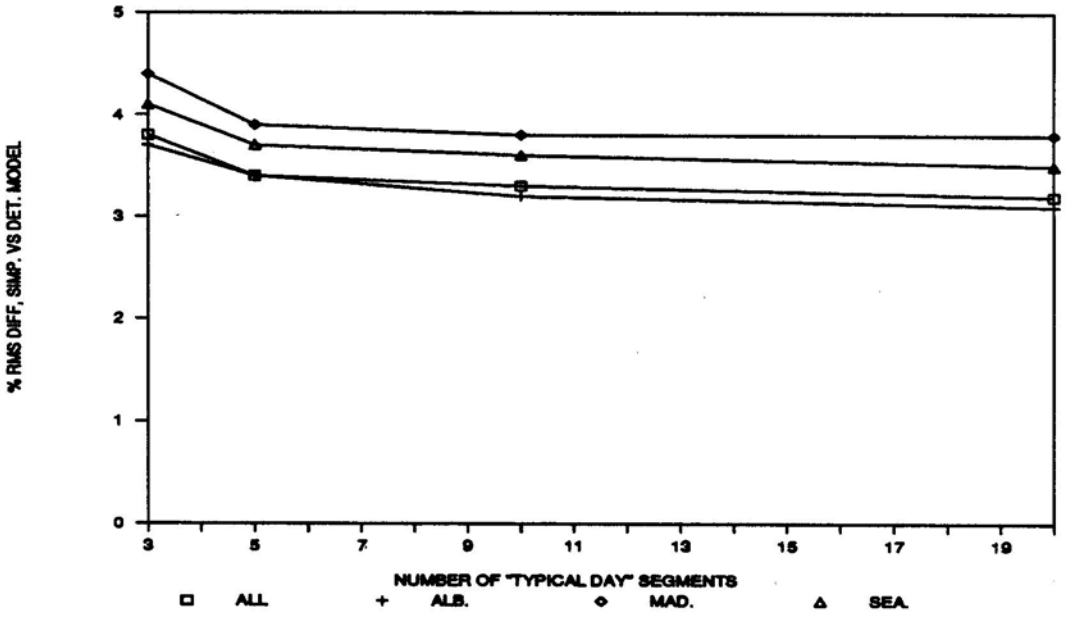

Figure 58. Annual % RMS vs. # of "Typical Day" Segments

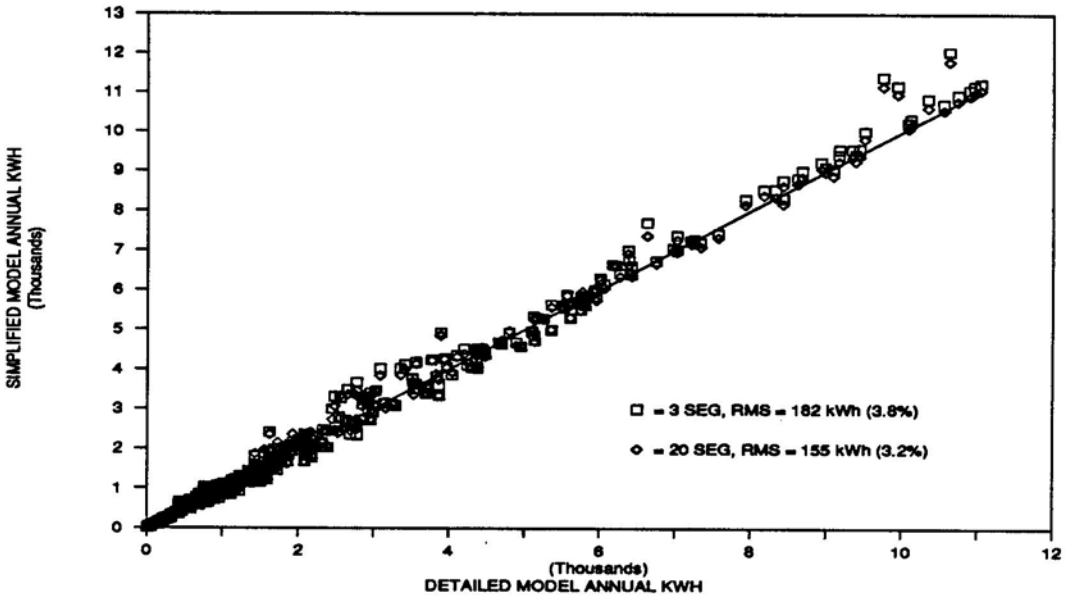

Figure 59. Predicted Annual kWh, DCPVSIMP VS. DCPVDET

The data shown in Figure 59 do not identify which types of cases tend to have large differences with respect to the detailed model's predicted performance. Figure 60 provides more information on the sources of error in the DCPVSIMP model. The y -axis is a plot of the percentage difference in annual output between the 3 segment DCPVSTh1P model and the DCPVDET model for 816 cases. These points are plotted against the corresponding annual direct-coupled effectiveness (direct-coupled kWh/max power-tracked kWh) for each case, as predicted by the DCPVDET model. There is a funnel shaped relationship between the percentage error and the effectiveness. Similar plots for the 5, 10, and 20 segment versions are not shown - the shape is similar, but the distribution is narrower. Cases which have a low annual effectiveness are not a characteristic of certain locations or load types, but rather, can occur for any case in which there is a poor match between the array and the load.

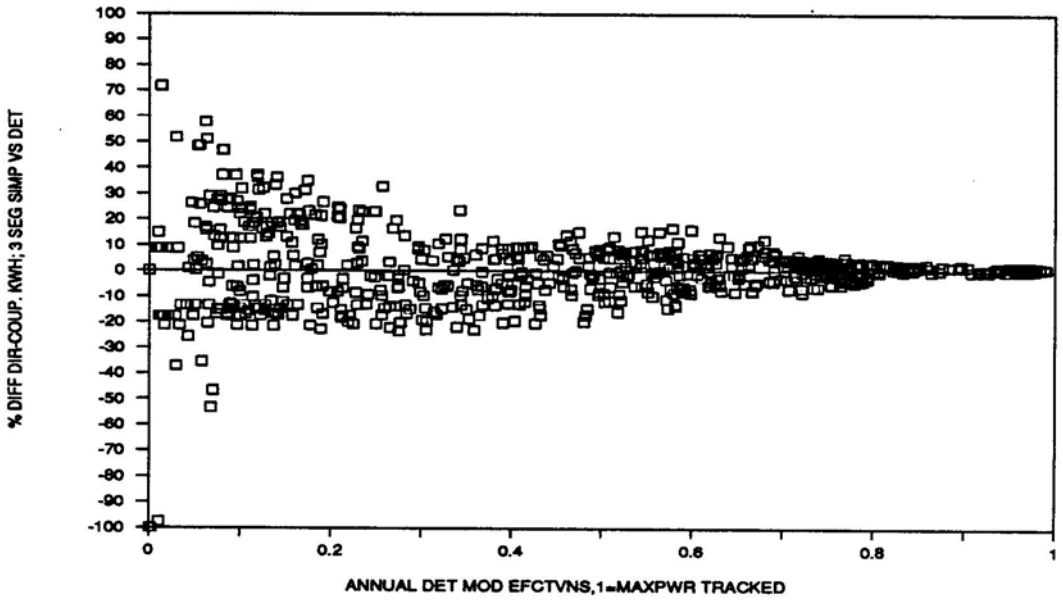

Figure 60. 3 Seg. Simp. Model % Diff. vs. Det. Model Effectiveness

Poorly matched resistive loads have either a much higher resistance (a nearly horizontal load I-V line relative to the array I-V curve) or much lower resistance (i.e., nearly vertical load line) than the optimum resistance. Poorly matched fixed voltage loads will intersect the array I-V curve far from the maximum power voltage, or they may even exceed the array open circuit voltage. There have been numerous examples of poorly matched motor/pump loads reported [37.41.42]. An obvious case is when the motor starting current is higher than the array current and none of the array's potential power is extracted. Figures 61, 62, and 63 separate the points from Figure 60 into fixed voltage, resistive, and pumping loads. The funnel shape is most apparent from the pumping load plo4 but this is because there are a wider variety and greater number of these cases. The process of defining the cases was both patterned and arbitrary; a larger number and wider variety of very poorly matched resistive and fixed voltage loads could also have been selected.

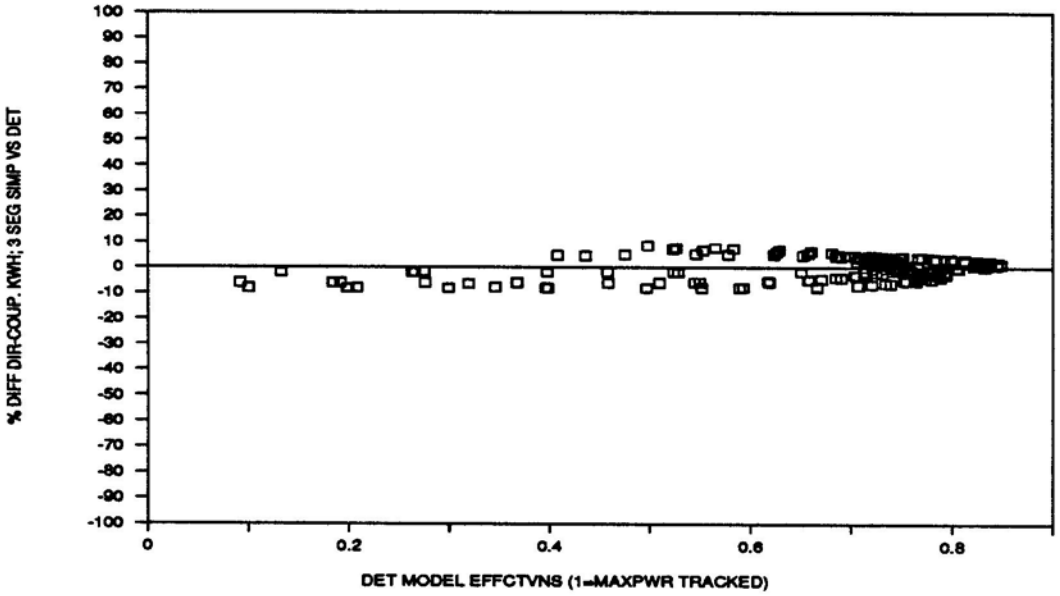

Figure 61. Fixed Voltage Loads: 3 Seg. Simp. Model % Diff. vs. Det. Model Effectiveness

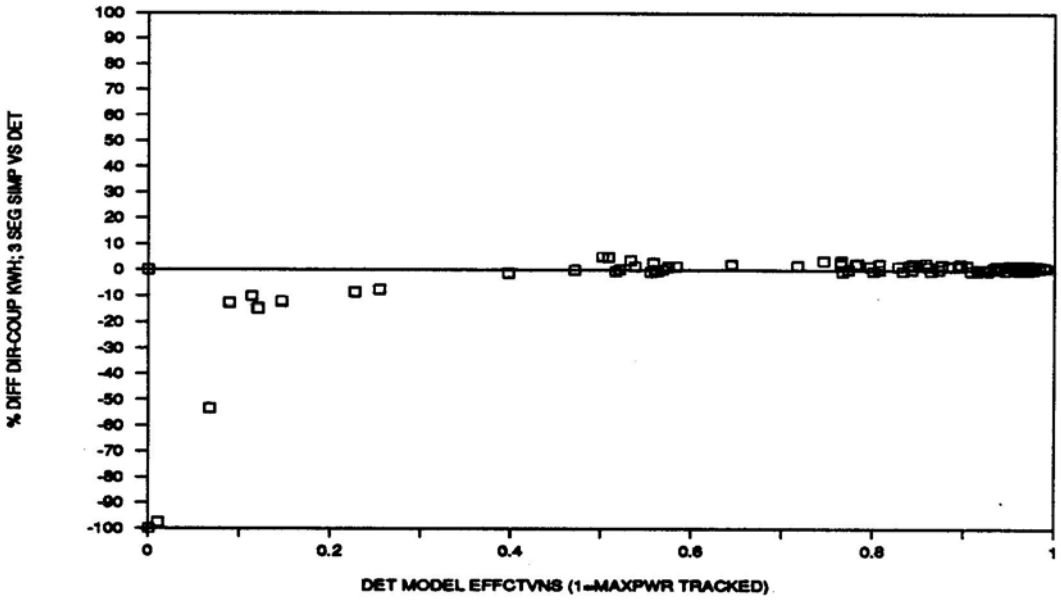

Figure 62. Resistive Loads: 3 Seg. Simp. Model % Diff. vs. Det. Model Effectiveness

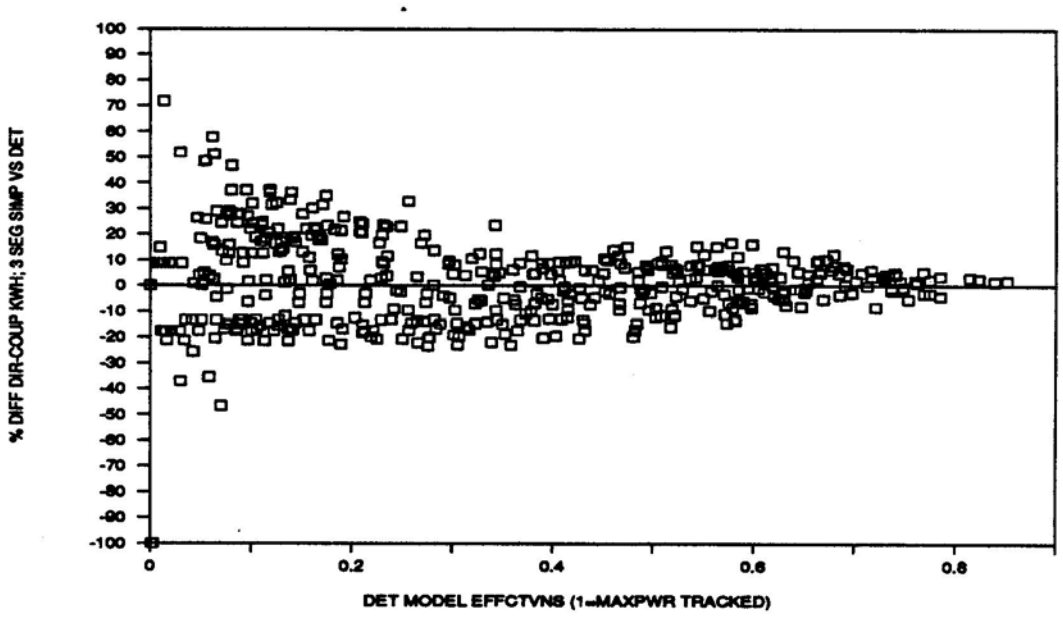

Figure 63. Pumping Loads: 3 Seg. Simp. Model % Piff. vs. Det. Model Effectiveness

Figures 60 - 63 indicate that the largest differences occur for cases in which the load and array are poorly matched. It is unlikely, given the present costs of PV technology, that designs as low as ≈60 - 70% effectiveness would be cost-effective. Therefore, the fact that an estimate with an effectiveness of 10% may be 50% off may not be significant. It is more important to identify ways to improve the direct-coupled effectiveness and obtain more confident results.

Figures 60 - 63 do not indicate whether the magnitude of the differences in the annual energy estimates are important. For example, a large percentage difference may not be significant if the projected kWh difference is small. Figure 64 is a plot of the kWh

difference between the simplified and detailed models versus the detailed model effectiveness. Taken alone, this plot is misleading - it implies that there are many cases at low effectiveness with significant kWh differences, i.e., differences as large as those shown for high effectiveness cases. Therefore, companion Figure 65 is included, which shows the same Y -axis difference plotted against the total annual kWh forecast by the detailed model. This figure shows that for most of the low effectiveness cases, the kWh differences are still small relative to the annual energy output.

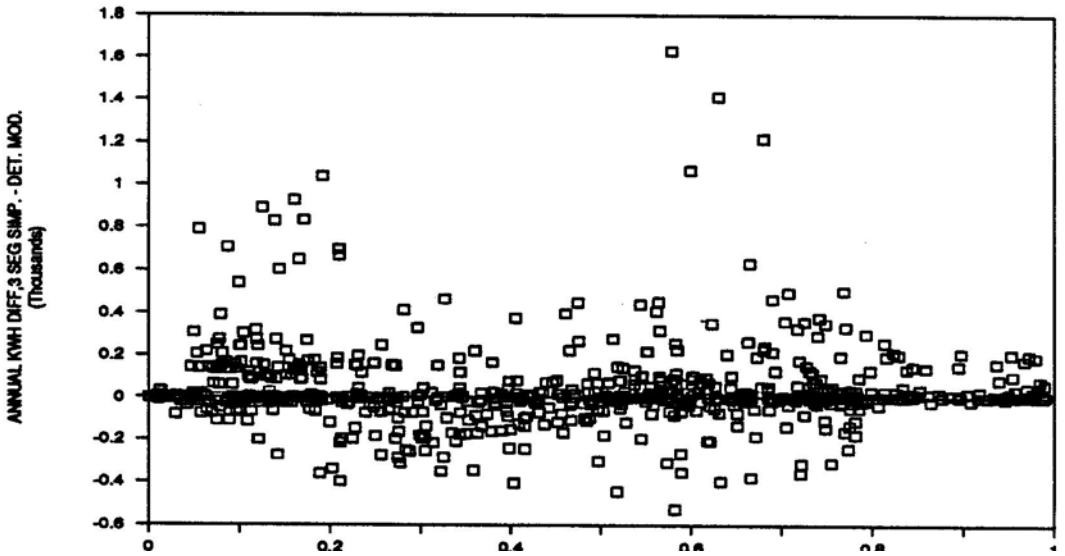

Figure 64. Annual Predicted Energy Difference vs. Detailed Model Effectiveness

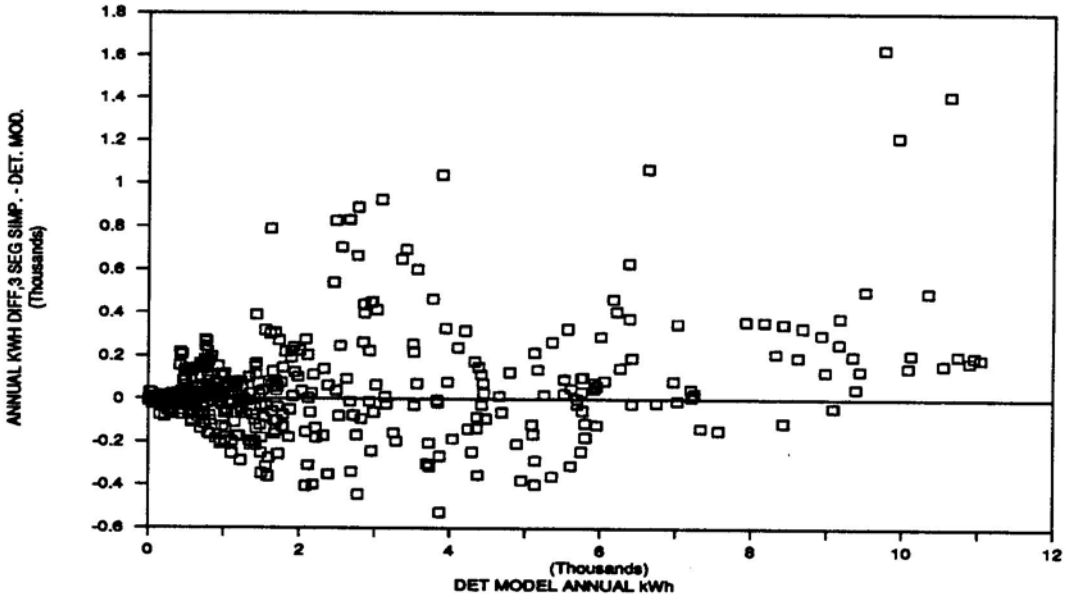

Figure 65. Annual Predicted Energy Difference VS. Detailed Model Output

Figure 60 implies that the accuracy of the DCPVSIMP model improves as the effectiveness of the design increases. Figure 66 and Table 14 show the variation in % RMS difference between the simplified and detailed models as cases of increasing effectiveness are removed from the sample. When 169 cases of less than effectiveness are removed from the original sample of 816 cases, the % difference for the 5 segment simplified model increases slightly, from 3.4% to 3.6%. This is because concentrations of points close to zero error are among the 169 cases omitted. When an additional 157 cases are removed with effectiveness below 30%, the % RMS difference drops to 3.0%, and when a total of 616 cases are removed with effectiveness below 70%, the % RMS difference drops to 1.4%. None of the original 816 cases had an effectiveness of 100%, so an actua11imiting % RMS difference has not been calculated (the sample size and the % RMS difference both approach zero). As an approximation to this limit, the overall % RMS difference for maximum power-tracking systems (100% effectiveness) is about 0.4%.

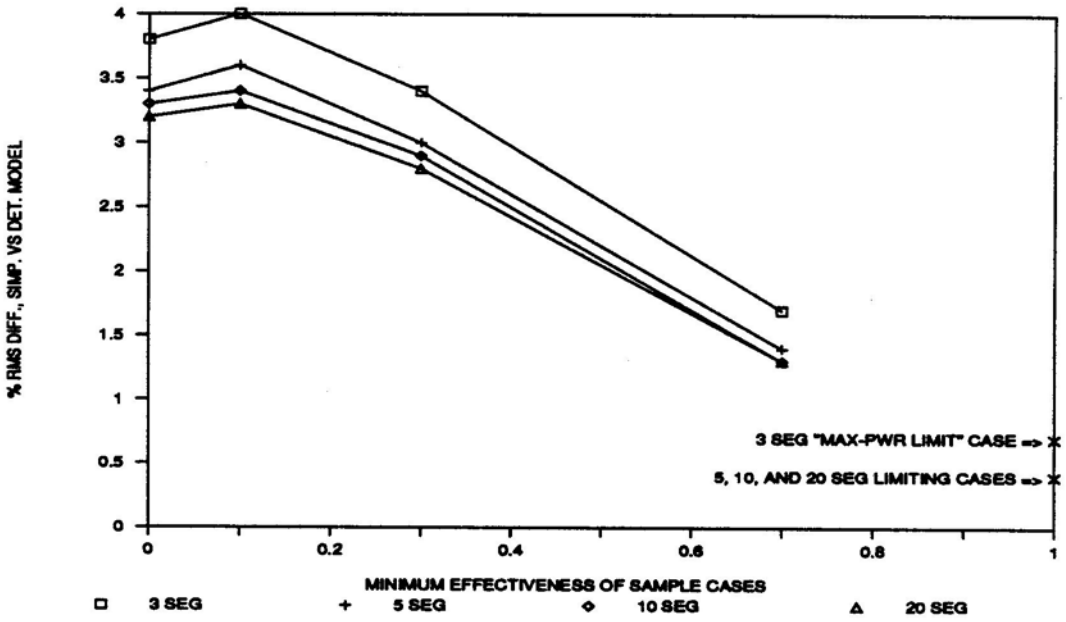

Figure 66. Change in % RMS Difference by Removing Low Effectiveness Cases

Table 14. DCPVSIMP V5. DCPVDET: Annual % RMS and % MBD with Low Effectiveness Cases Removed.

DCPVSIMP # segs. =>	3	5	10	20
% RMS, All 816 cases	3.8	3.4	3.3	3.2
% RMS. 647 cases> 10% err.	4.0	3.6	3.4	3.3
% RMS. 490 cases >30% err.	3.4	3.0	2.9	2.8
% RMS, 200 cases >70% eff.	1.7	1.4	1.3	1.3
Limiting % RMS for max power-tracking, 816 cases	0.7	0.4	0.4	0.4
% MBD. All 816 cases	0.7	0.5	0.4	0.4
% MBD. 647 cases > 10% err.	0.7	0.5	0.4	0.3
% MBD, 490 cases >30% err.	0.4	0.3	0.1	0.1
% MBD, 200 cases >70% err.	0.5	0.2	0.1	0.0
Limiting % MBD for max power-tracking, 816 cases	0.3	0.1	0.0	-0.1

Figure 67 shows how the choice of effectiveness "cut-off" point affects the % MBD. A limiting value of the % MBD, when all cases approaching 100% effectiveness are removed, is approximated by the % MBD for maximum power-tracking systems.

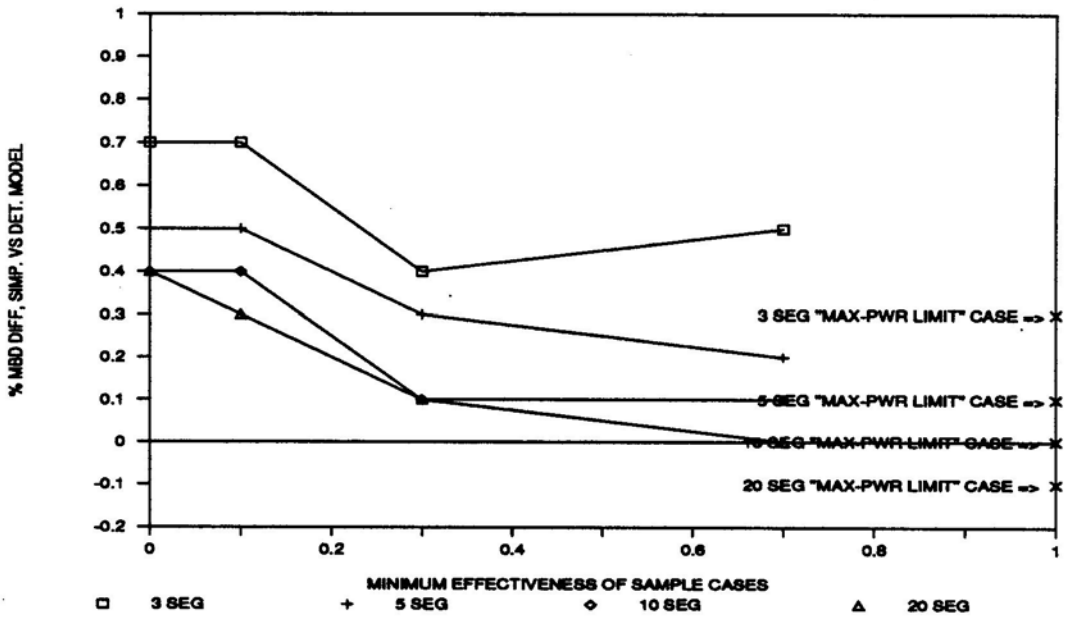

Figure 67. Change in % MBD Difference by Removing Low Effectiveness Cases

6.2.2 January and July Results

Another factor to check in evaluating the DCPVSIMP model is whether its accuracy is influenced by monthly weather variations. January and July results for each location have been selected to represent extremes of poor and good weather. Figures 68 (January) and 69 (July) are plots of the direct-coupled kWh output predicted by the 3

segment and 20 segment versions of the simplified model versus the corresponding output predicted by the detailed model. There is more scatter than for the annual results shown in Figure 59. Figures 70 (January) and 71 (July) are plots of the percentage difference in output between the 5 segment simplified model and the detailed model versus the detailed model effectiveness. Even though data from the 5 segment version is shown on these plots, the funnel shape is wider than for the 3 segment annual data shown in Figure 60. Tables 15 and 16 summarize the January and July results, respectively, for the same 816 cases discussed in the previous section. These results are also broken down by location.

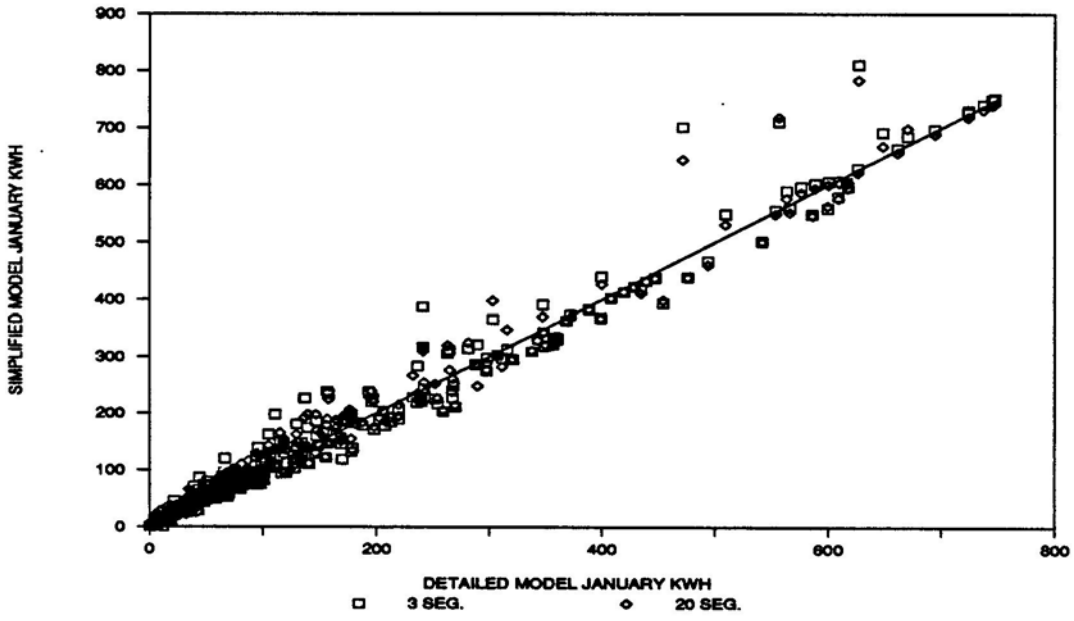

Figure 68. Predicted January kWh, DCPVSIMP vs. DCPVDET

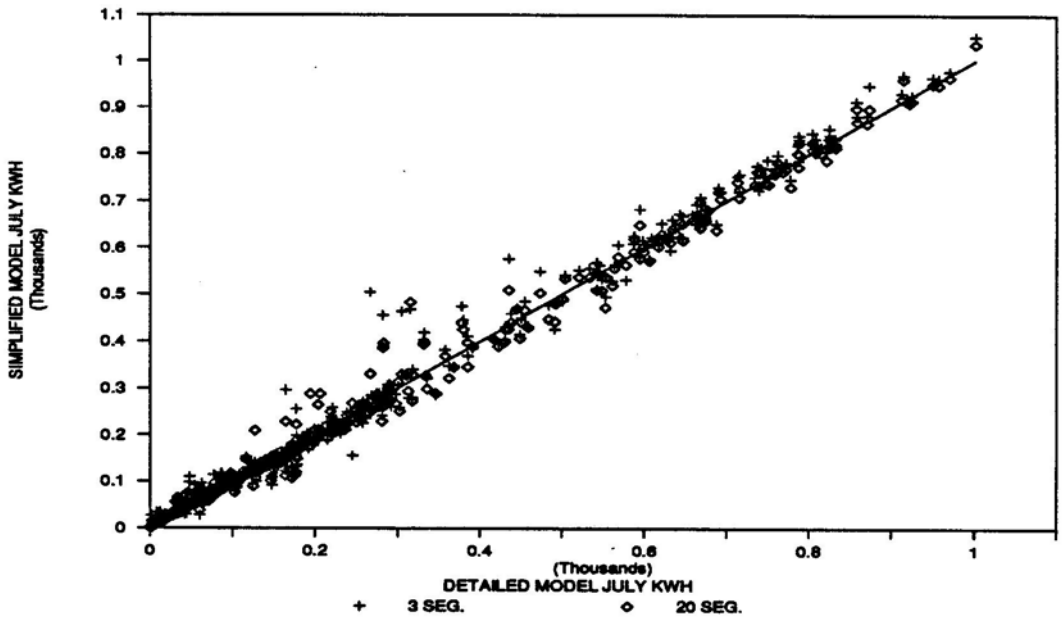

Figure 69. Predicted July kWh, DCPVSWP vs. DCPVDET

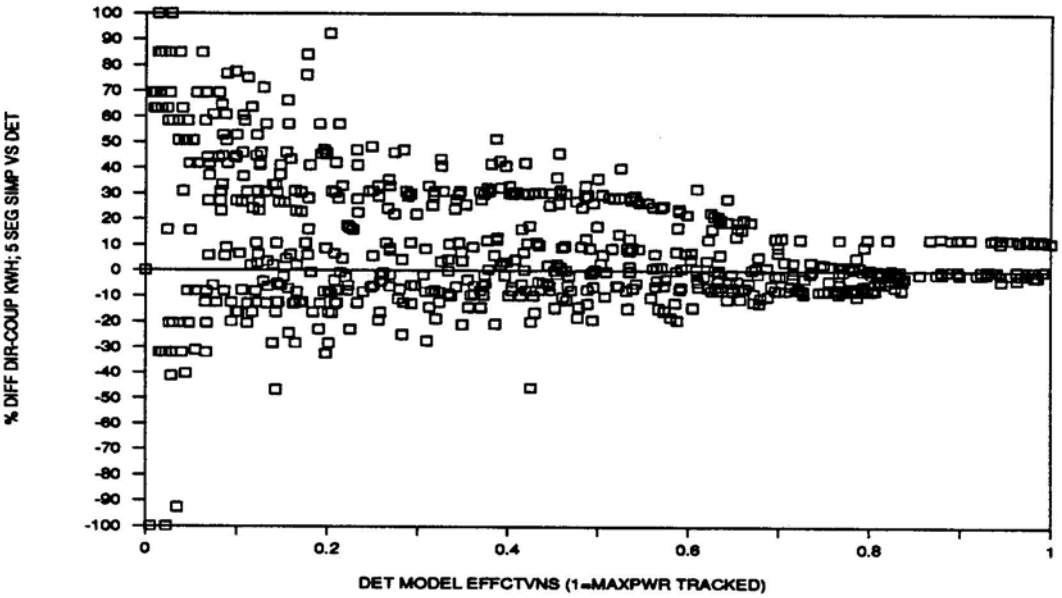

Figure 70. January: 5 Seg. Simp. Model % Diff. vs. Bet. Model Effectiveness

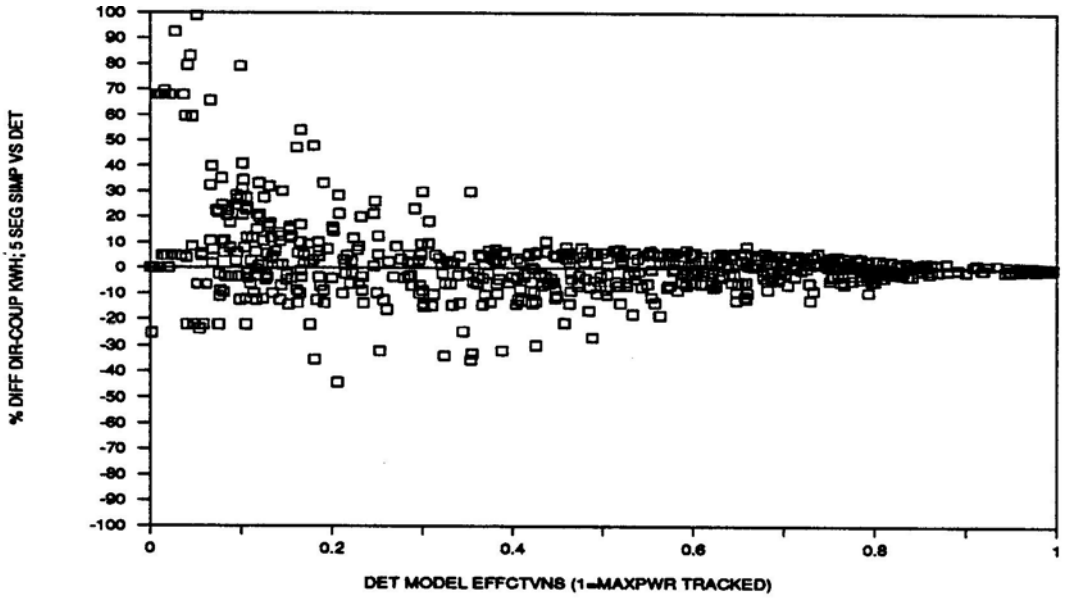

Figure 71. July: 5 Seg. Simp. Model % Diff. vs. Del Model Effectiveness

Table 15. DCPVSIMP vs. DCPVDET: % RMS and % MBD, January Summary

DCPVSIMP # segs. =>	3	5	10	20
All cases, % MBD	0.7	0.7	0.7	0.7
All cases, % RMS	6.0	5.4	5.3	5.1
All cases, RMS kWh	19	17	17	16
Albuq. % MBD	1.1	-0.2	-0.4	-0.5
Albuq. % RMS	7.1	6.3	6.1	5.9
Mad.%MBD	-0.7	1.2	1.1	1.0
Mad % RMS	5.5	5.0	4.8	4.2
Sea. % MBD	4.3	5.9	6.7	6.9
Sea. % RMS	11.8	11.3	13.3	12.9

Table 16. DCPVSIMP vs. DCPVDET: % RMS and % MBD, July Summary

DCPVSIMP # segs. =>	3	5	10	20
All cases, % MBD	0.7	0.3	0.1	0.0
All cases, % RMS	4.6	3.6	3.5	3.5
All cases, RMS kWh	23	18	17	17
Albuq. % MBD	0.8	0.5	0.3	0.2
Albuq. % RMS	4.3	4.3	4.2	4.1

Mad.%MBD	0.5	0.1	-0.1	-0.1
Mad % RMS	4.1	2.3	2.3	2.4
Sea. % MBD	0.7	0.2	-0.1	-0.1
Sea. % RMS	5.5	3.5	3.4	3.5

Figure 72 compares the % RMS differences for the monthly and annual results, as a function of the number of segments used in the simplified model, and Figure 73 compares .the % MBD. The % MBD results are inconclusive because the differences are so minor, but the % RMS results show that the model is less accurate for January or July than it is for the annual estimates. This seasonal variation in accuracy is due to a similar inaccuracy in one or more of the correlations used to generate weather-dependent variables.

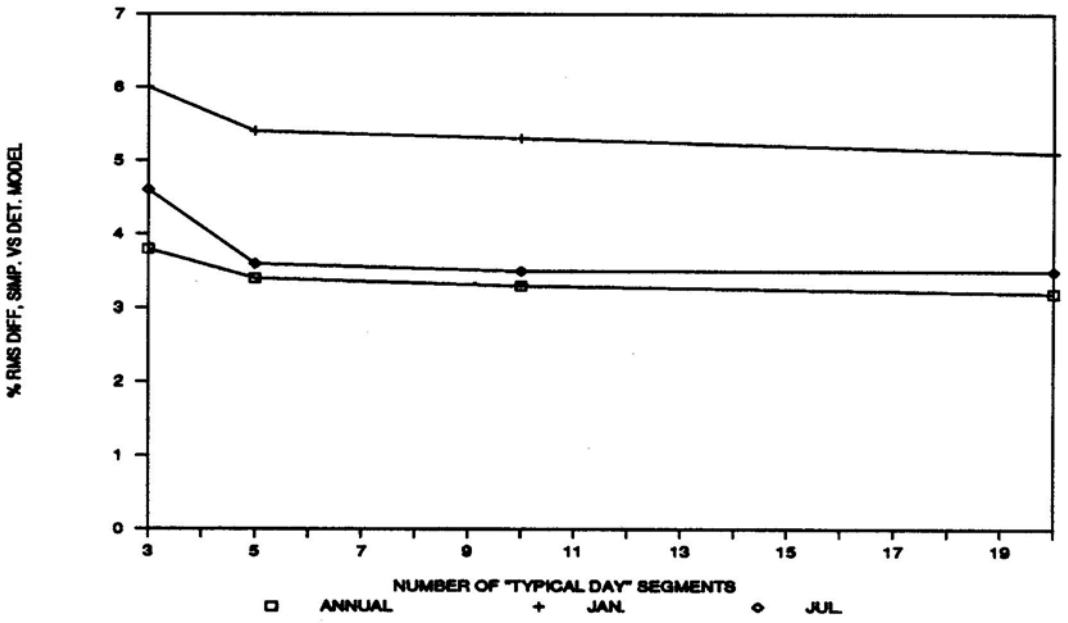

Figure 72. January, July and Annual % RMS Diff. vs. # of Segments

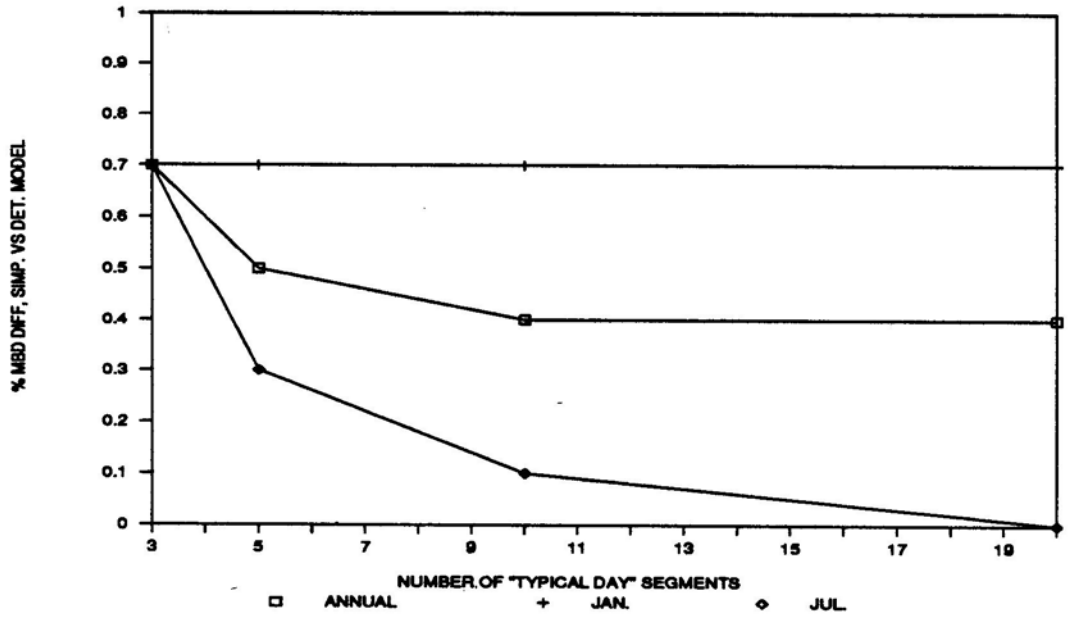

Figure 73. January, July and Annual % MBD Diff. vs. # of Segments

Referring to Tables 13, 15, and 16, there is a wider variation in accuracy between locations during January than during July or over the year. The Seattle results are the most sensitive, with % RMS differences that increase from 11 to 13% as the number of segments increases from 3 to 20. One explanation is that the monthly-average clearness index for Seattle in January is very low (about 0.3), and the Bendt correlation may be inaccurate at low K_t's. However, for Albuquerque, the % RMS difference for January is also higher that the annual average, and this location has a January clearness index of about 0.62. It may be that the daily KT distributions have a distinct "stair-step" shape that the Bendt correlation replicate or the TMY data for one month may not be representative of the long-term statistic embodied in the Bendt correlation. It is also possible that the seasonal inaccuracies may be due to poor estimates of average geometric variables such as daylength, declination, and/or incidence angles.

6.3 System Design Applications for the DCPVSIMP model

The following series of plots use results from a variety of cases based on the 5 segment version of the DCPVSIMP model. The plots are intended to show the sensitivity of various performance measures (e.g., effectiveness, kWh output, or volume of water pumped) to factors such as location, month, module type, series/parallel arrangement, and load type.

These types of plots can be used to help optimize direct-coupled system designs. As shown in Section 6.2.1, some results may be inaccurate for cases with a low predicted effectiveness, i.e., below about 50%, but this should not change the designer's decision process on how to obtain improved designs. The sensitivity curves can still be used to

steer toward optimal designs, and good confidence (about 3% or less RMS error) can be had for designs of 70% effectiveness or better.

Each of the following three sections presents results for a different load type: either fixed voltage, resistive, or motor loads.

6.3.1 Fixed Voltage Loads

Highly effective direct-coupled designs can be obtained with fixed voltage loads, but the designs are strongly sensitive to the choice of load voltage. Figure 74 is a plot of the predicted monthly kWh from a 500 W (nominal peak rating) ARCO array as a function of the direct-coupled load voltage. Curves are shown for two months, January and July, at each of three locations: Albuquerque, Madison, and Seattle (tilt = latitude for each case). The optimum load voltage is primarily a function of cell temperature, and the cell temperature is primarily a function of ambient temperature and irradiance. Low cell temperatures, and therefore, high optimal voltages, are characteristic of locations with cold ambient temperatures and low solar radiation, i.e., Madison in January. The optimum voltage is about 20% lower for locations with high ambient temperatures and/or high solar radiation, such as Albuquerque or Madison in July. At 230 volts, this array would produce about the same energy at Madison in January as it would at Albuquerque in July - less than half of what it could produce at Albuquerque in July.

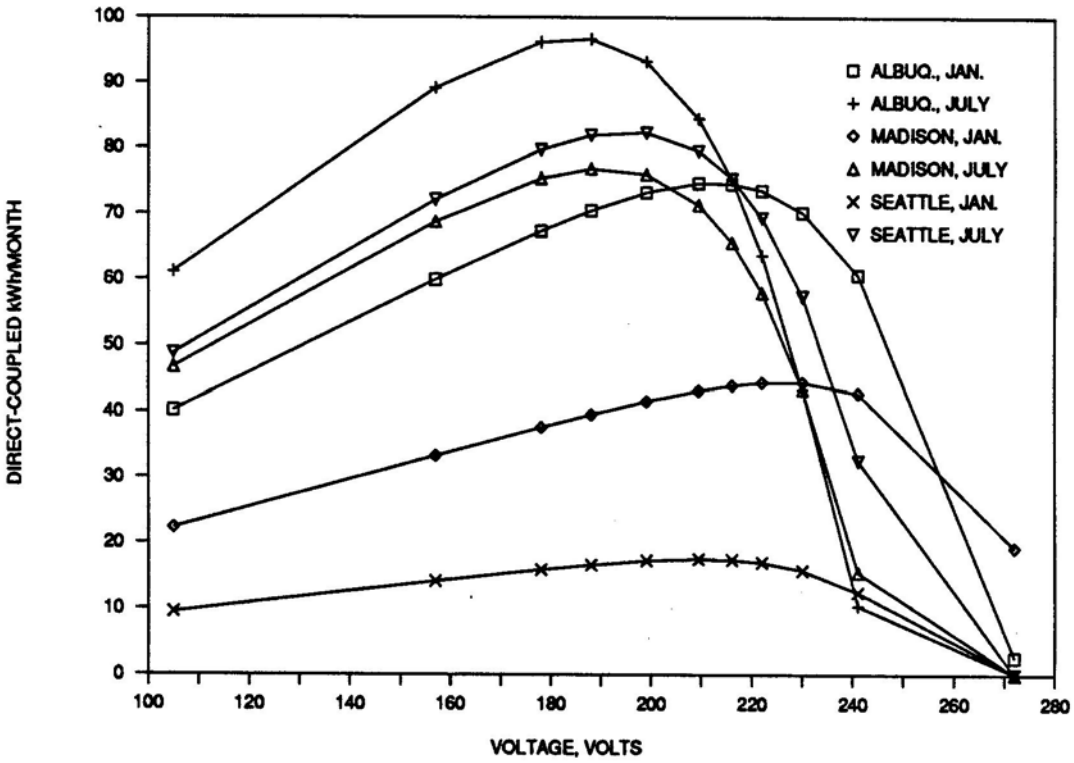

Figure 74. 500 W ARCO Array: Monthly kWh Output vs. Voltage

Figure 75 shows how the effectiveness varies with load voltage. This plot is based on the same array as the previous plot. However, the results are non-dimensiona1ized so that they may apply to any size array of similar quality, or fill factor. fill factor, FF, is equal to the maximum power divided by the product of the circuit current and open circuit voltage.) January, July, and annual average effectiveness curves are shown for Albuquerque and Seattle. These curves show the sharp drop in effectiveness for load voltages which exceed the optimum voltage. They also show that at the proper voltage, as much as 99% of the energy obtainable with maximum power-tracking may be extracted (ignoring losses in the maximum power-tracker, typically about 5%).

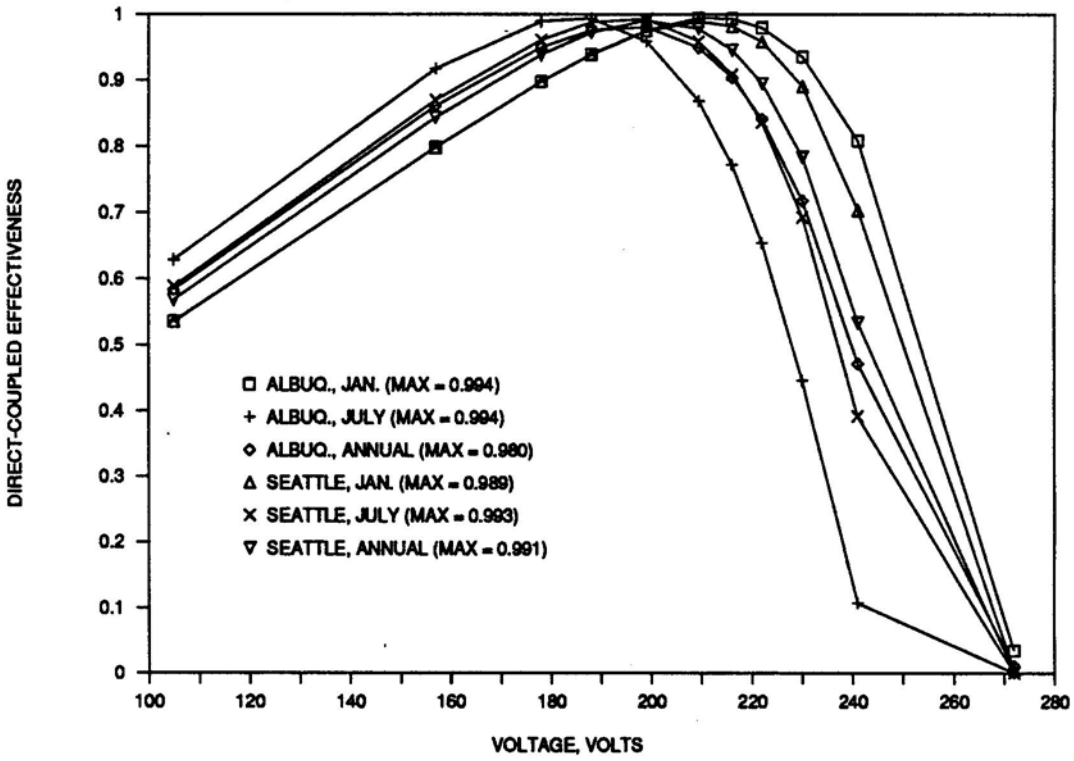

Figure 75.500 W ARCO Array: Effectiveness vs. Voltage

Figures 76 and 77 non-dimensionalize the voltage scale by normalizing the load voltage relative to the monthly optimum voltage. With both axes non-dimensionalized, comparisons among arrays of different sizes and voltages are possible. Three types are compared here: A 30 W, 12 V Solarex module; a 500 W, 180 V ARCO array; and a 4500 W, 180 V Tri-Solar array. For both the January data shown on Figure 76 and the July data shown on Figure 77, the curves are similar, except that the array with the poorest fill factor (ARCO) is least sensitive to non-optimum voltages, while that with the best fill factor (Solarex) tends to show a narrower and steeper dependence on the voltage ratio.

This is because the Power- Voltage characteristic of a system with a poor fill factor is less peaked than one with a high fill factor. If the optimum monthly voltage could be reliably estimated, it appears that a correlation could be developed relating the effectiveness, voltage ratio, and perhaps fill factor. The factors of season or location do not appear to be significant.

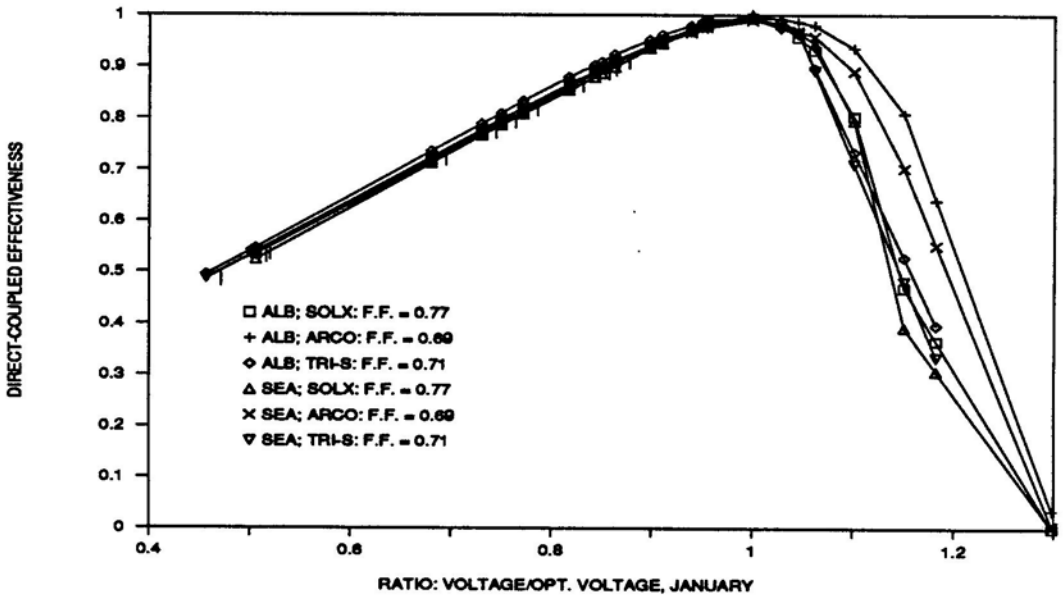

Figure 76. Effectiveness vs. Voltage Ratio for 3 Systems in January at 2 Locations

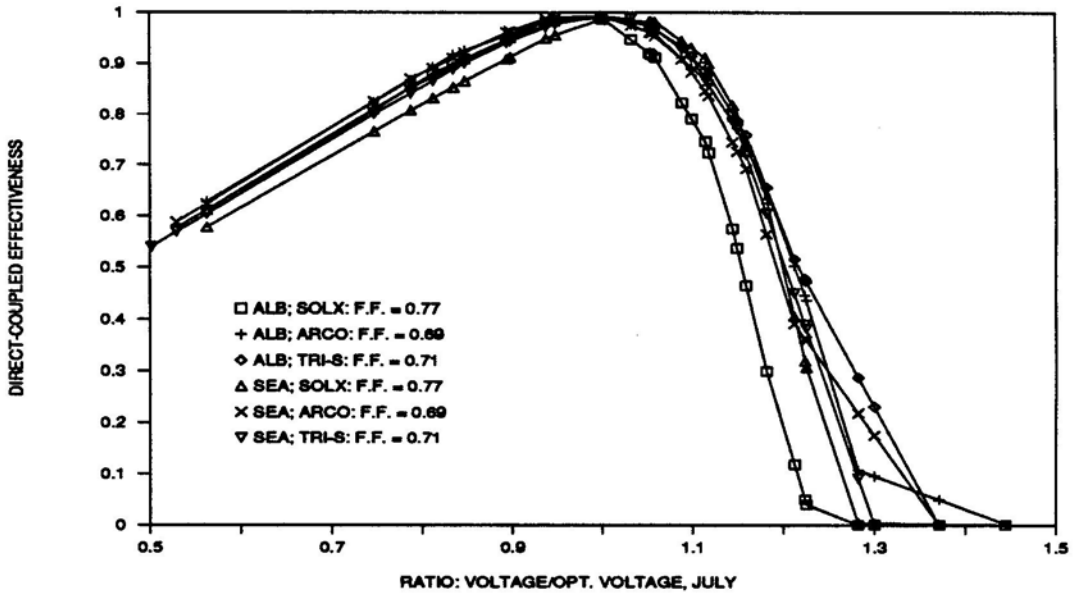

Figure 77. Effectiveness vs. Voltage Ratio for 3 Systems in July at 2 Locations

Figures 78 and 79 show how the array energy and effectiveness vary by month for three choices of fixed voltage. The same 500 W ARCO array as modeled in the previous examples is used, and the array is located in Madison. The three fixed voltages correspond to the optimum voltages for either January, July, or the year. For reference, a fourth curve is included on Figure 78 which shows the maximum power-tracked system energy production. These figures demonstrate that if a single load voltage must be fixed. it is better to design the system to match at the summer conditions. The effectiveness penalty is severe in the summer months if the system is designed to match well under winter conditions, but the opposite is not true; the system energy production tracks the maximum fairly closely at all times of the year when the July optimum voltage is used.

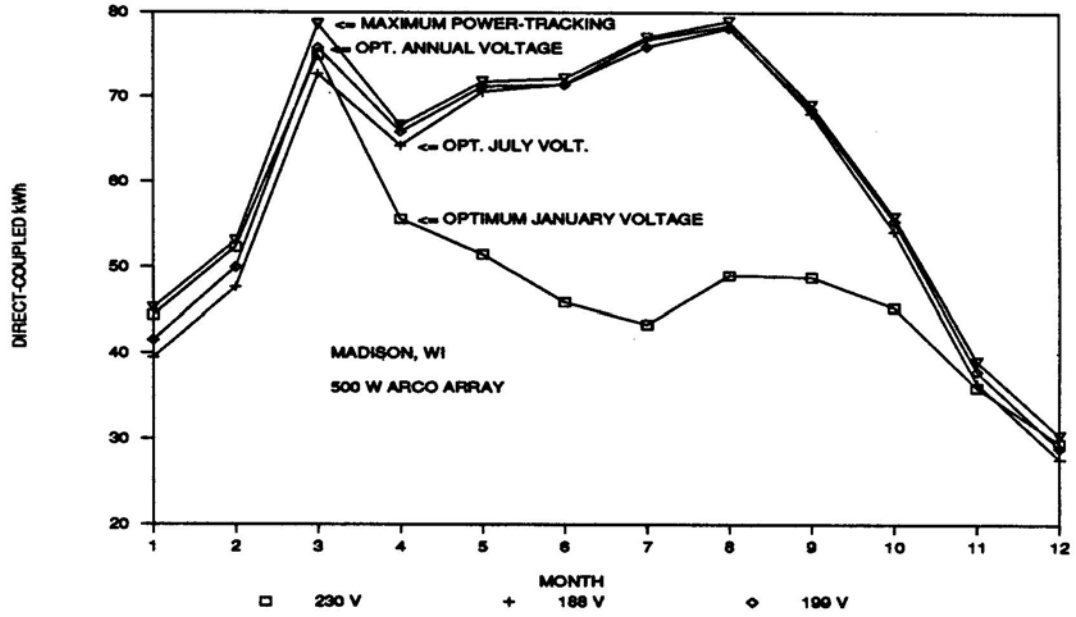

Figure 78. Estimated Monthly Energy Production for a 500 W ARCO array in Madison

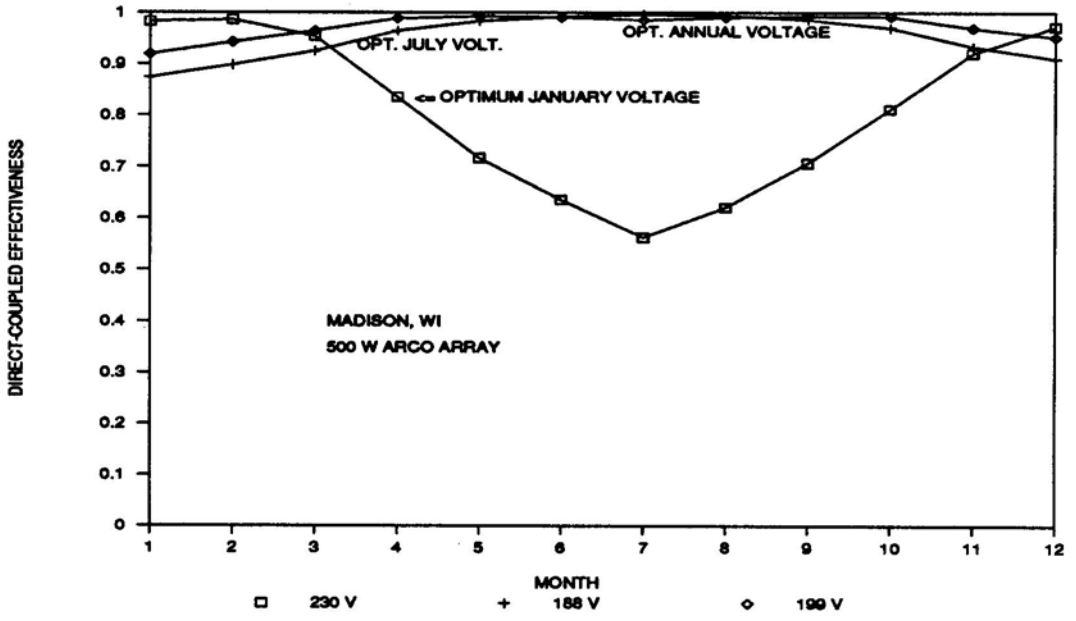

Figure 79. Estimated Monthly Effectiveness for a 500 W ARCO array in Madison

6.3.2 Resistive Loads

Unlike fixed voltage loads, fixed resistance loads cannot be direct-coupled to achieve near-maximum performance. This is because the optimum resistance at any instant is nearly a function of irradiance, and the irradiance typically varies by about three orders of magnitude over each day. The effect of temperature on the optimal resistance is relatively insignificant compared to the effect of irradiance.

Figure 80 shows the estimated monthly kWh from a 500 W ARCO array for January and July at Albuquerque, Madison, and Seattle (tilt = latitude for each case). The optimum resistance increases as the average solar radiation decreases. These curves indicate that for design purposes it would be better to err on the high side of the optimum resistance, because of the steep drop in output for resistances less than the optimum. For a design using one fixed annual resistance, this would indicate that the winter performance should dictate the choice of resistance, as opposed to fixed voltage loads, where the load/array voltage should be based on summer optimum conditions. However, a tradeoff exists because the solar radiation is much greater in summer than in winter. A case study illustrating this tradeoff is presented later in this section.

On Figure 81, the Y -scale of Figure 80 is non-dimensionalized in terms of the direct-coupled effectiveness, but all other variables are unchanged. This plot demonstrates that regardless of the choice of fixed resistance, on a monthly basis, the optimum effectiveness is substantially less than that possible with a fixed voltage load - about 80%, compared to 95% or better for fixed voltage loads. This plot also shows that for an extremely poor month such as Seattle in January, the effectiveness is not sensitive to resistances greater than the optimum value.

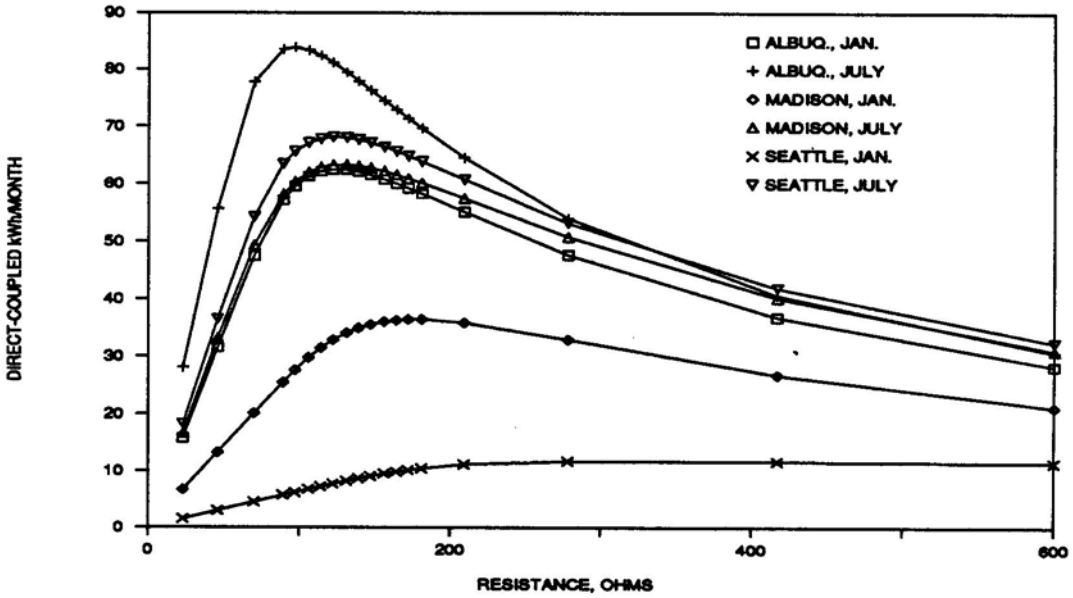

Figure 80. 500 W ARCO Array: Monthly kWh Output vs. Resistance

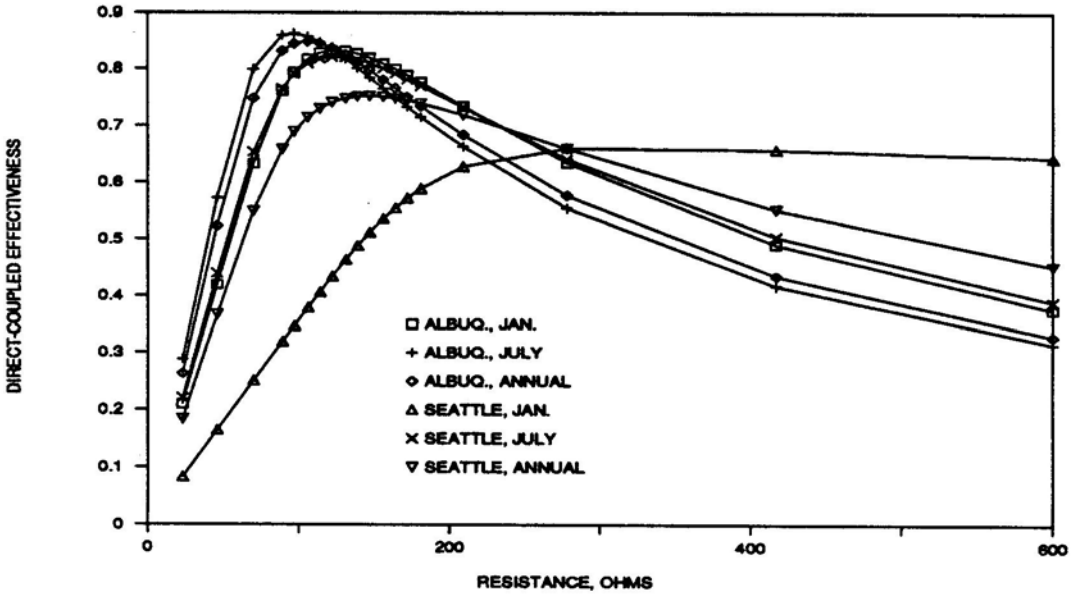

Figure 81. 500 W ARCO Array: Effectiveness vs. Resistance

Figure 82 is designed to show the effects of monthly-average radiation and array type on the monthly direct-coupled effectiveness, over a range of resistances. The resistance scale is non-dimensionalized relative to the January optimal resistance for each of the four system configurations shown. These curves indicate that the radiation, as quantified by the monthly-average clearness index, has a significant effect on the effectiveness-resistance ratio relationship. They also show the lesser effect that the array type, as quantified by the fill factor, has on the effectiveness-resistance ratio relationship.

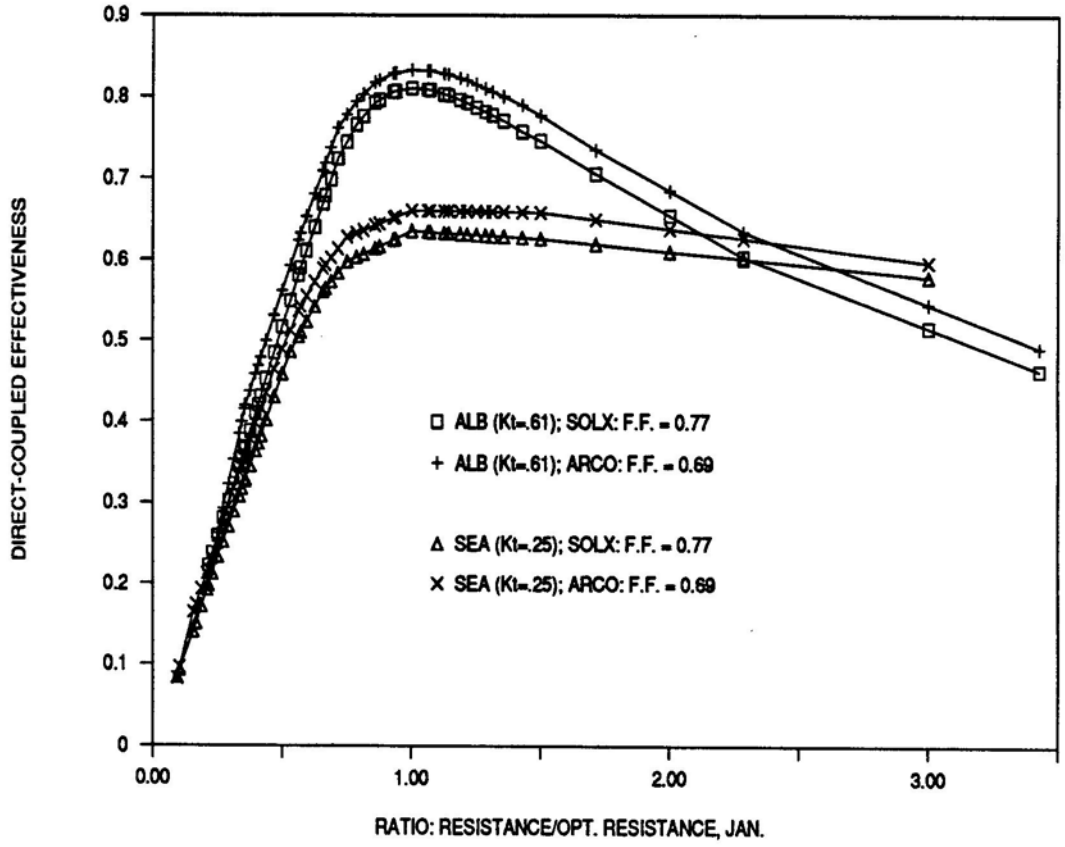

Figure 82. Effectiveness vs. Resistance Ratio for 2 Systems in January at 2 Locations

Figure 83 compares the optimum direct-coupled effectiveness for 18 system configurations, including the four shown in Figure 82. The 18 systems are made up of 3 arrays x 3 locations x 2 months at each location. The monthly-average clearness indices are listed for each location/month combination, and the fill factors characteristic of each array type are listed above the legend. There appears to be a distinct although not linear, relationship between the effectiveness at the optimal resistance (i.e., the "best-possible" performance) and the monthly-average clearness index, the performance increasing with clearness index. As noted on Figure 82, the optimum effectiveness also appears to be weakly related to the fill factor, with the optimum effectiveness increasing as the fill factor decreases. This is not to imply that the poorer quality arrays (i.e., low fill factor) are capable of greater performance. The higher effectiveness attainable from the poorer quality array is a consequence of the fact that the poorer quality array has a broader maximum power range. The maximum power output, however, is less than that which could be extracted from a similarly sized array with a higher fill factor.

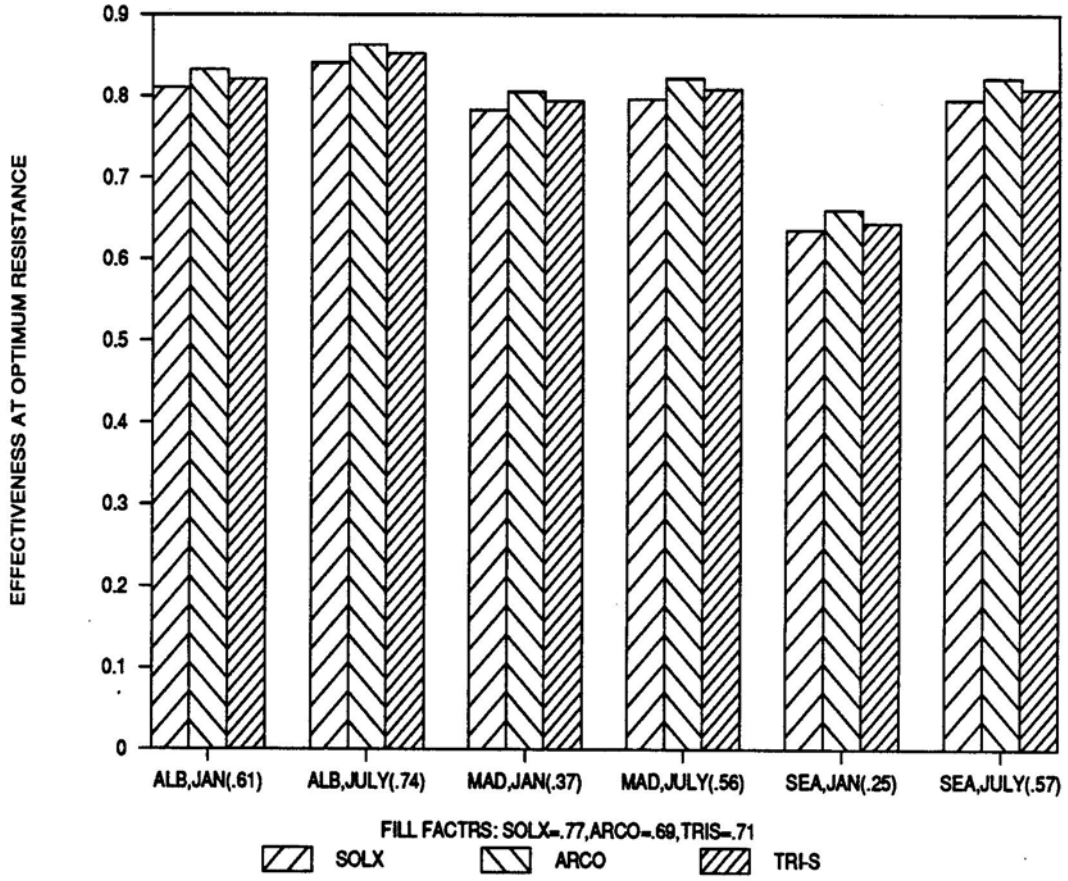

Figure 83. Optimum Effectiveness for 18 Resistive Cases

Analogous to the curves shown for fixed voltage loads (Figs. 76, 77), if an optimum monthly resistance can be estimated beforehand, then it may be possible to develop a correlation between effectiveness and resistance. Having such a correlation would eliminate the need to do lengthy simulations to estimate long-term performance.

Although this subject has not been investigated thoroughly, it has been hypothesized by the author that the optimum monthly resistance may be estimated by the following expression, which accounts for array-dependent and radiation-dependent

characteristics, but ignores temperature, diffuse energy, and geometric orientation effects.

$$R_{LOAD,OPT} \approx \frac{V_{MAX,REF}}{I_{MAX,REF}} \cdot \frac{\Phi_{REF}}{(\overline{K}_T) \cdot G_{SC}} \tag{6.6}$$

Figures 84 and 85 show how the array energy and effectiveness vary by month for three choices of fixed resistance. The same 500 W ARCO array as modeled in the previous examples is used, and the array is located in Madison. The three fixed resistances corresponding to the optimum resistances for either January, July, or the year. For reference, a fourth curve is included on figure 84 which shows the maximum power-tracked system energy production. At all times of the year, the direct-coupled system produces substantially less electricity than a comparable maximum power-tracked system. These figures demonstrate that if a single fixed load resistance is used, it is advantageous to design the system to match at the summer conditions. Unlike with the fixed voltage load, however, the annual performance penalty is not severe if the system is designed for optimum performance under winter conditions.

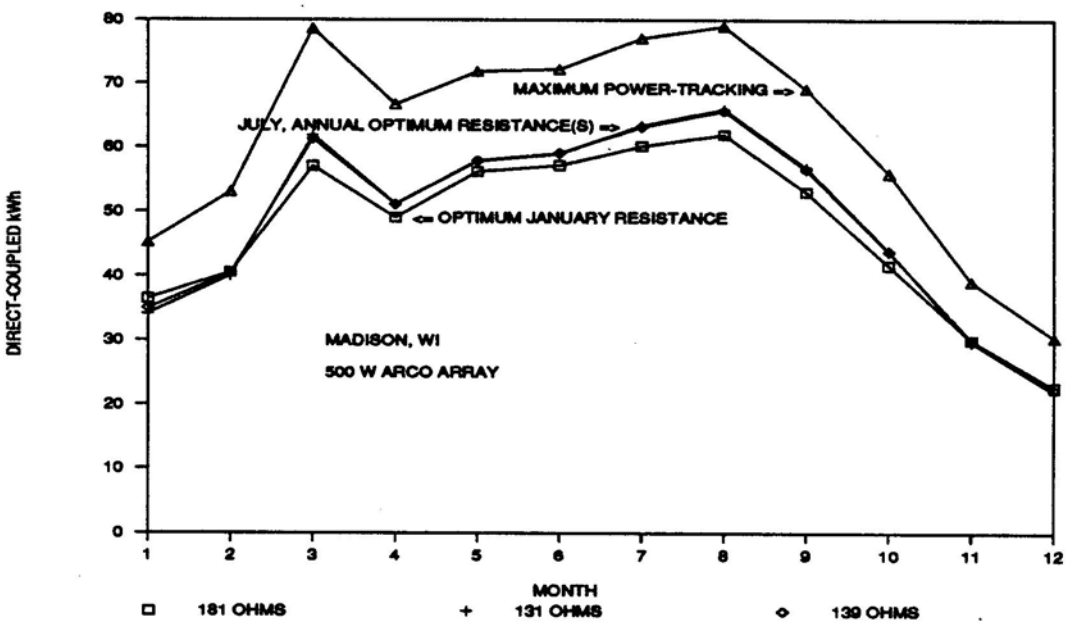

Figure 84. Estimated Monthly Energy Production, Resistive Loads

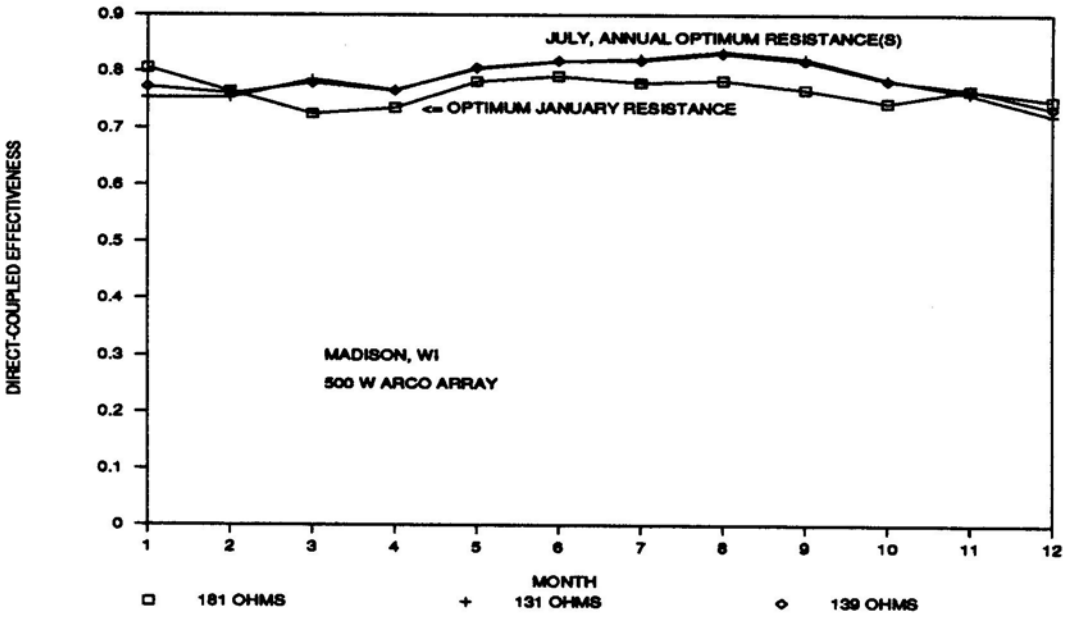

Figure 85. Estimated Monthly Effectiveness. Resistive Loads

6.3.3 Motor Loads

It is more difficult to present generalized performance comparisons for motor loads because of the non-linear I-V characteristics of the many varieties of motors and because each motor's I-V characteristic is influenced by the mechanical torque and speed characteristics of the load it is serving.

For a given load, the designer must select from a variety of DC motors of comparable size, taking into account factors such as maintenance requirements, reliability, and cost (such factors are not considered in this study), in addition to mechanical characteristics such as rated power, efficiency, torque, and speed range. Figures 86 - 88 compare the annual performance of three types of comparably sized DC motors connected to the same load. The three types considered are series, permanent magnet, and shunt DC motors, each rated at about 1000 W. The load is a centrifugal ventilator fan, the torque and speed characteristics of which were given in Section 3.3.4.1. The motor parameters and motor/load I-V characteristics are listed in Appendix A, and I-V plots for each motor/load are shown in Sections 3.3.1 - 3.3.3. The motor/load combinations are direct-coupled to an array of 30 W Solarex modules. The annual performance was estimated for 49 different array configurations ranging from 1 to 15 modules in series and in parallel, each located in Madison at a tilt equal to the latitude.

Figure 86 is a 3-D plot of the annual effectiveness of the series motor-based system for each of the 49 array configurations. The contour lines above each plot are spaced at increments of 0.05 effectiveness. A maximum effectiveness of 0.67 occurs for a

system of 7 parallel and 5 series modules. This plot qualitatively illustrates the importance of matching the array and load I-V characteristics by using a proper combination of series and parallel modules. In this case, the effectiveness drops sharply for greater than 7 series modules and 7 parallel modules, with poor performance also estimated for any combination of less than 5 modules in parallel.

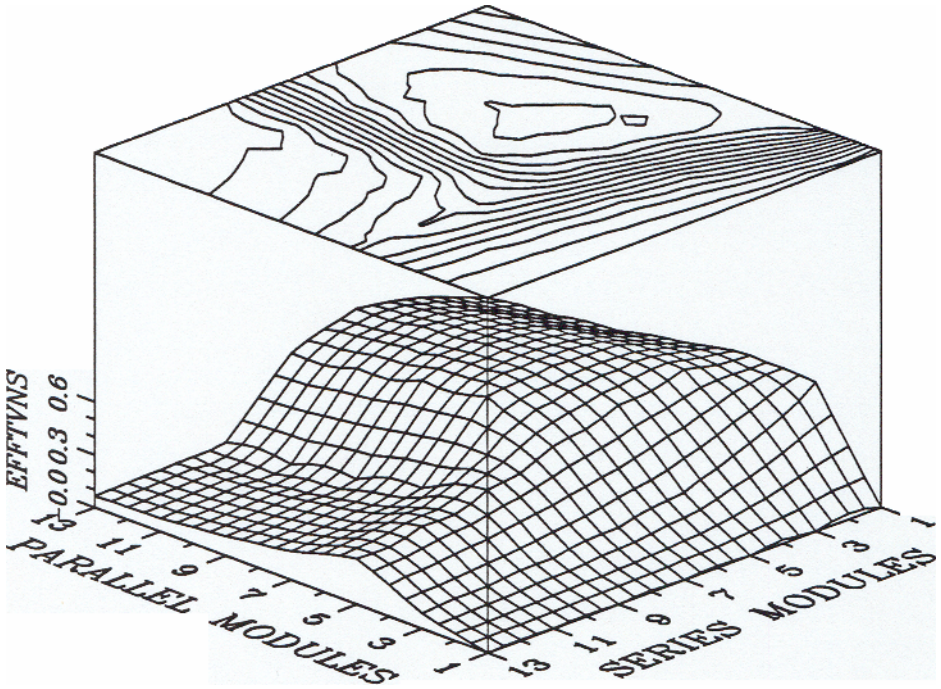

Figure 86. Variation in Effectiveness for Arrays of 30 W Solarex Modules, Series Motor, and Centrifugal Fan Load, in Madison

Figure 87 is a corresponding plot of annual effectiveness for a permanent magnet motor-based system. A maximum of 0.79 occurs for a system of 5 parallel and 7 series modules. Better performance is indicated for smaller arrays of either 1 x 1,2 x 2, or 3 x 3 in series/parallel than for the series motor, and this may be attributed to the permanent magnet motor's lower starting torque characteristic (Section 3.3.3, Figure 38), which enables the system to operate at lower currents than for the series motor-based system.

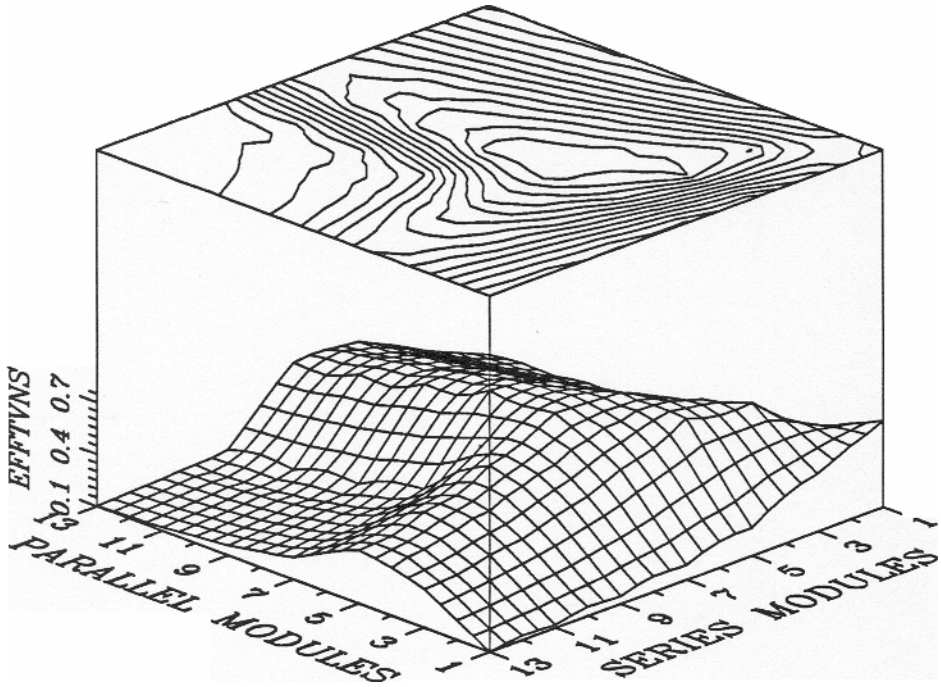

Figure 87. Variation in Effectiveness for Arrays of 30 W Solarex Modules, Permanent Magnet Motor, and Centrifugal Fan Load, in Madison

Figure 88 shows the variation in effectiveness for a shunt motor-based system. This system is notably poorer for most configurations and achieves a maximum effectiveness of 0.59 for an an-ay of 11 parallel and 1 series module(s). The high starting torque characteristic of this type of motor requires a large number of modules in parallel

to generate enough current to start the motor.

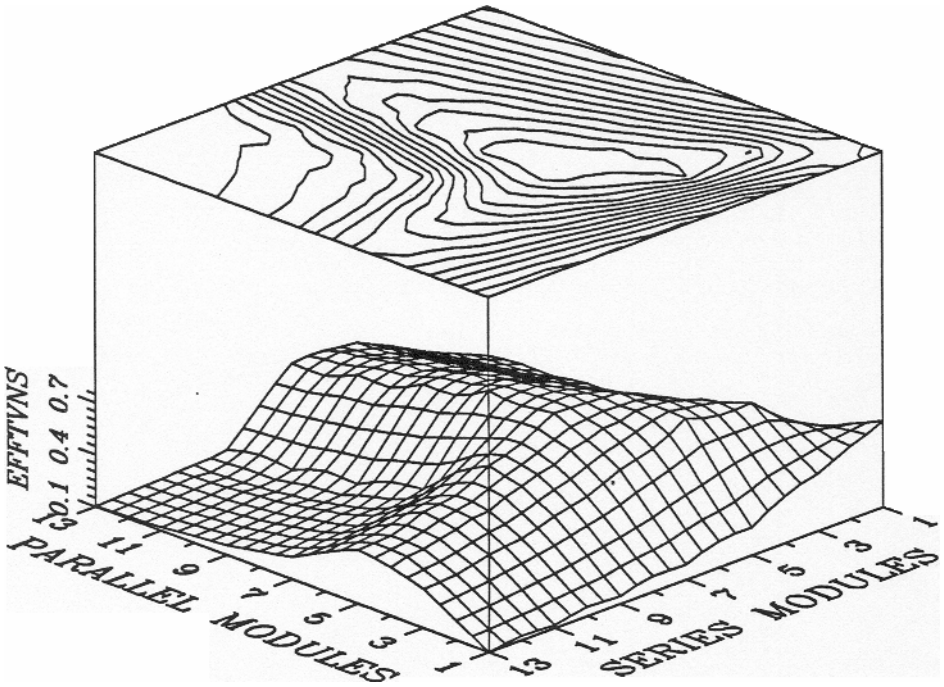

Figure 88. Variation in Effectiveness for Arrays of 30 W Solarex Modules, Shunt Motor, and Centrifugal Fan Load, in Madison

Plots of this type show how the DCPVSIMP model may be used to help select a proper series/parallel configuration and motor type in order to optimize annual performance for a given load, location, and module type. For this example, an array of 5

parallel and 7 series Solarex modules direct-coupled to the permanent magnet motor yields the best annual effectiveness. For other locations, the relative performance may differ.

Figures 89 and 90 show how the optimum array configuration varies for each type of motor at three locations (tilt = latitude). The optimum annual effectiveness is plotted on the Y -axis of Figure 89 and the corresponding annual kWh is plotted on the Y-axis of Figure 90. Effectiveness may not be the quantity of greatest importance for some applications. These plots illustrate how the most effective choice of array and motor may not provide the greatest output among the range of design options. as is the case with the series vs. permanent magnet motor comparison for both Albuquerque and Seattle.

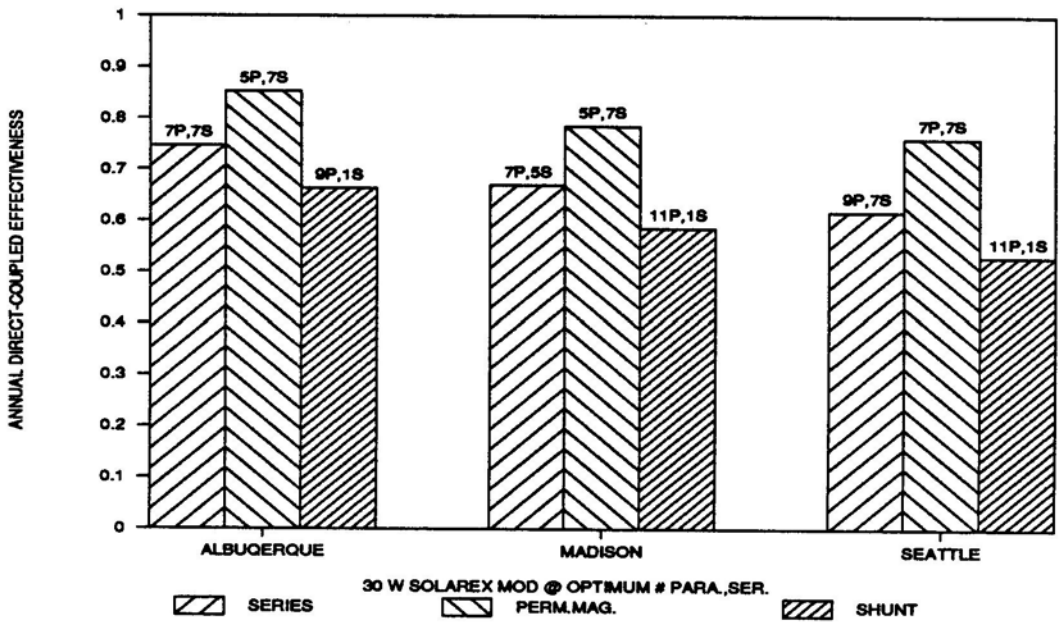

Figure 89. Variation in Effectiveness for Optimal Arrays of 30 W Solarex Modules for 3

Motors and 3 Locations

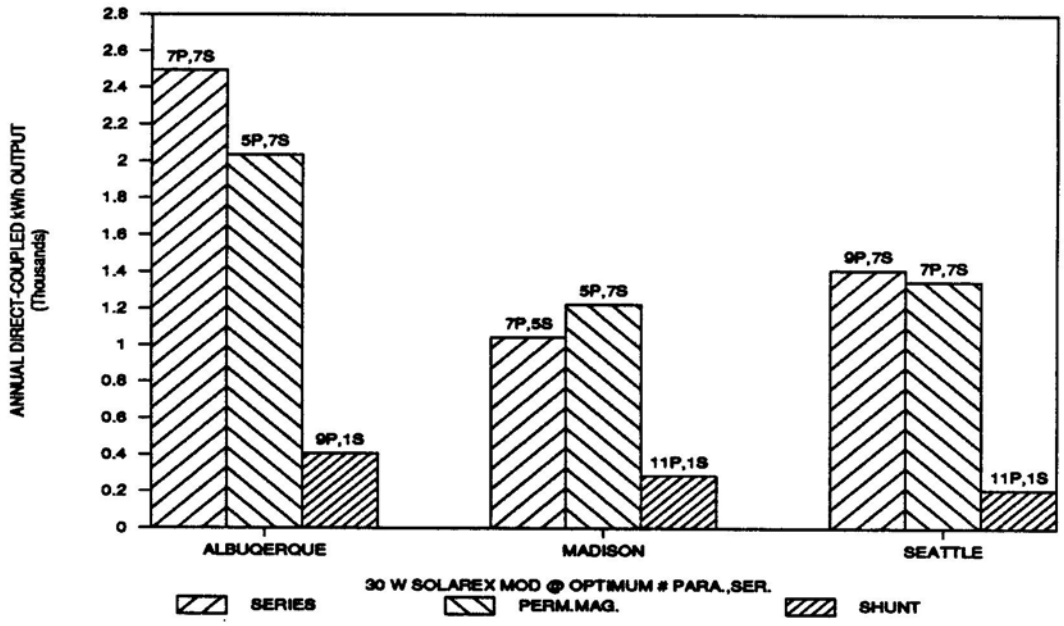

Figure 90. Variation in Annual kWh Output from Optimal Arrays of 30 W Solarex Modules for 3 Motors and 3 Locations

Figure 91 compares the estimated performance of a 5000 W series motor-based system and a 5000 W permanent magnet-based system used to run a centrifugal water pump in Albuquerque (tilt = latitude). The water pump's characteristics are shown in Figure 40 of Section 3.3.4.2. Cases were run for either 1 or 2 PV units in series, and between 1 and 15 units in parallel. The basic PV unit modeled is a 500 W array, which is itself built up of several ARCO 40 W modules.

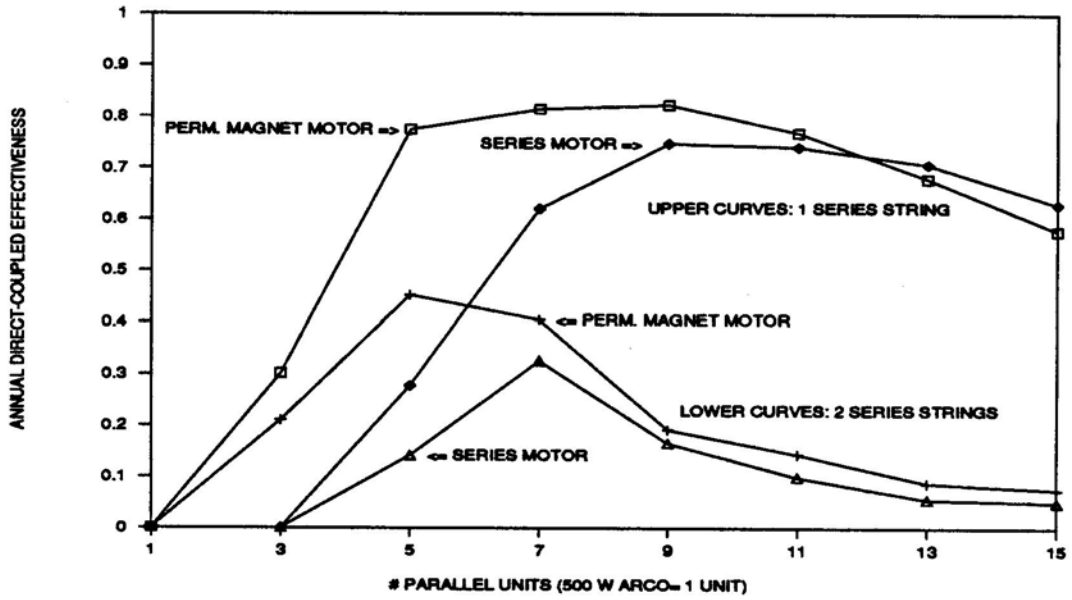

Figure 91. Variation in Annual Effectiveness for Multiples of a 500 W ARCO array. for 2 Motors. at Albuquerque

A relatively broad optimum of about 80% exists around 9 parallel and 1 series multiples of the 500 W unit, with a significant effectiveness advantage for the permanent magnet motor. The effectiveness vs. number of modules in parallel curve is also overlaid on the composite Figure 92, which also shows the variation in pumped water volume and in kWh generated by the array. These curves only apply for 1 series string and for the permanent magnet motor-based system. The electricity generated and water pumped continue to increase with the number of units in parallel beyond the peak effectiveness. However, the total output begins to decrease when the array becomes so large that the motor maximum speed is exceeded even at low radiation levels, so that the hours of operation are progressively reduced.

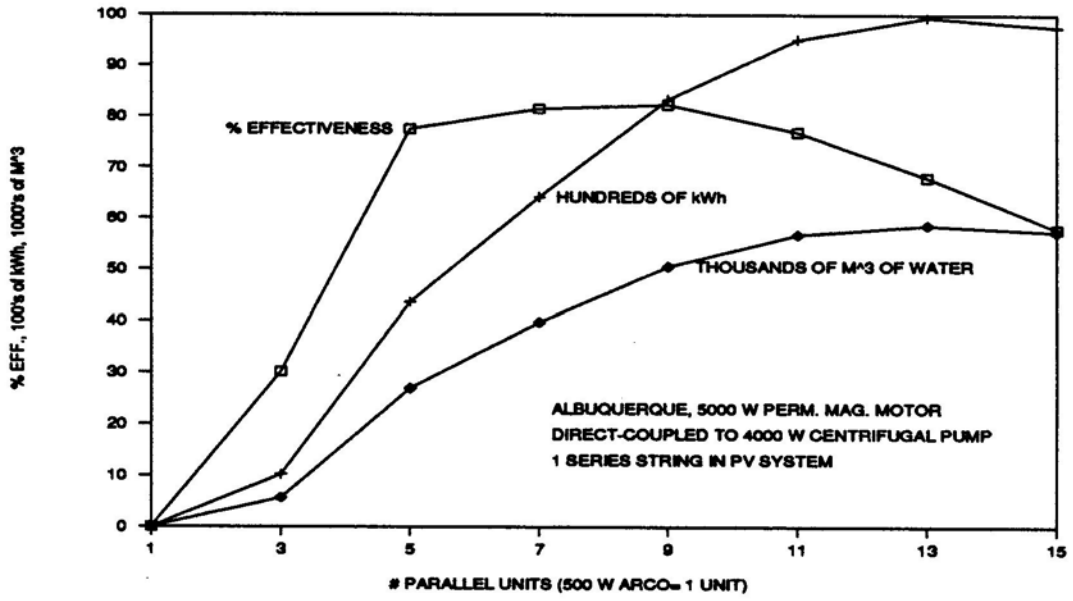

Figure 92. Effectiveness, kWh, and Water Pumped for Parallel Multiples of a 500 W ARCO an-ay, Permanent Magnet Motor, and Centrifugal Pump, at Albuquerque

The monthly variation in cubic meters of water pumped in Albuquerque is shown in Figure 93 for the optimum annual configuration of both the series and permanent magnet motor-based systems (9 parallel and 1 series). The permanent magnet motor-based system exhibits a consistent advantage over the comparably rated series motor for all months. The flattening of output experienced by both systems in the summer months is partly due to high ambient temperatures in the summer months and partly because October and the late spring months in Albuquerque have a higher average clearness index than the summer months.

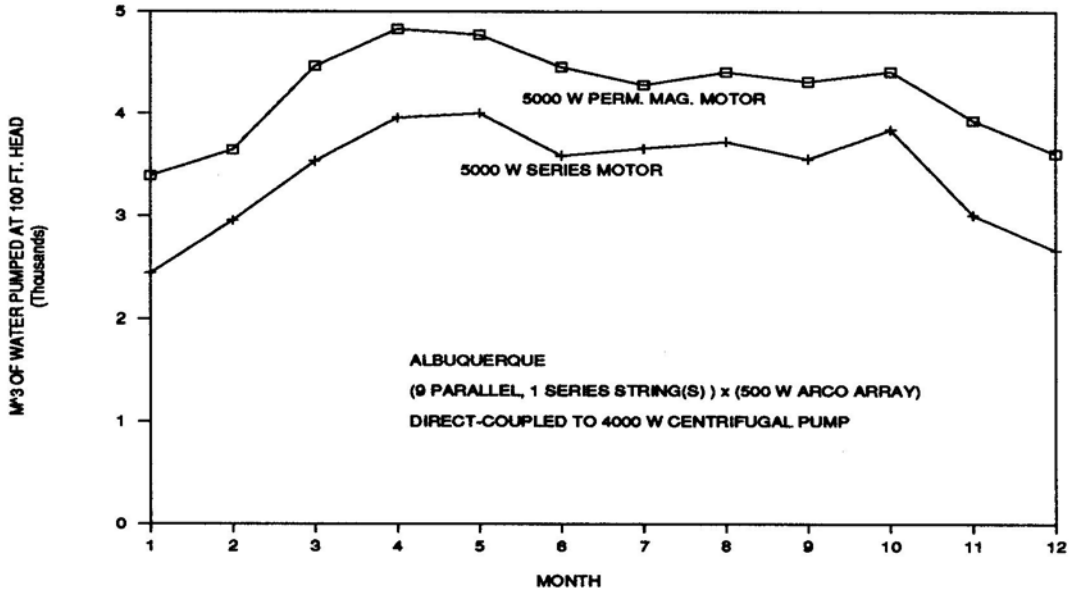

Figure 93. Monthly Water Pumped for 9 parallel x 1 series multiples of a 500 W ARCO array, Series and Permanent Magnet Motors, and Centrifugal Pump, at Albuquerque

6.4 Conclusions

The new DCPVSIMP (for **D**irect-**C**oupled **PV** model, **SIMP**lified version) model developed in this thesis uses a simplified method to estimate the long-term performance of direct-coupled and maximum power-tracked PV systems without battery storage. The DCPVSIMP model generates a reduced set of hourly weather-dependent variables from monthly-average weather data, then uses these to determine a PV array's hourly current-voltage (I-V) characteristics. It has been shown to have a monthly % root mean square (RMS) accuracy of about 5% and an annual RMS accuracy of better than 4% compared to a reference detailed model titled DCPVDET (for **D**irect-**C**oupled **PV** model, **DET**ailed version). This is within the ± 5 to 10% accuracy of the hourly Typical Meteorological Year ([MY) data used as input for the DCPVDET model.

The DCPVDET and DCPVSIMP models have also been found to be consistent with two established models, PV f-Chart [11] and PVFORM [12], for maximum power-tracked systems. The DCPVDET and DCPVSIMP models differ by less than 1 % for either monthly or annual results with maximum power-tracked systems. They differ from PV f-Chart by about + 5 to 6% and from PVFORM by ± 1 % over monthly or annual periods. The difference between PV f-Chart and the other models has been attributed to an incidence angle correction factor feature included in PV f-Chart but not in the other models.

The primary applications for the DCPVSIMP and DCPVDET models are for direct-coupled loads, such as resistive, fixed voltage, or other non-linear loads such as DC motors connected to pumps. Although long-tenD results have not been validated for these types of loads, there is good confidence in the models' accuracy because their critical component for calculating direct-coupled behavior, the array I-V sub-model, was found to correspond well (< 1% RMS difference) with experimental I-V curves.

The I-V curve sub-model uses an exponential equation with 4 parameters to describe the PV equivalent circuit, assumed to consist of a single lumped current source in parallel with a non-ideal diode, with an additional lumped apparent series resistance in series with the applied load. Ordinarily, just enough information can be obtained from PV manufacturer’s brochures to use a simpler 3 parameter equation, but long-term estimates using the 3 parameter equation for maximum power-tracked systems are generally biased

5 to 8% too low. A new analytical method has been developed in this thesis that permits use of an accurate an unbiased 4 parameter equation without requiring additional information.

Different versions of the DCPVSIMP model may be specified, depending on how many "typical day" segments are used to approximate the distribution of daily radiation within a month. Results from over 800 cases run with the DCPVDET model were compared to like results from the DCPVSIMP model using 3, 5, 10, and 20 "typical day" segments. The annual % RMS difference improved from about 4% to 3% when going from the 3 segment to 20 segment versions. The % mean bias differences were small (<1%) for each version. The conclusion is that in general, the 5 segment version is the most appropriate version to use for long-term estimates for any month and location.

One benefit of the DCPVSIMP model, especially with versions which use a small number of "typical day" segments, is its fast run time. Cases for PV f-Chart (<1 second for monthly and <5 second for annual results) and PVFORM (10.5 minutes for a "bare bones" case with no battery storage or economics calculations) were done on an IBM PC (with math co-processor), while comparable cases for the 5-segment DCPVSIMP (4-5 sec.) and DCPVDET (40-45 sec.) models were done on a Digital Equipment Corp. MicroVAX II. It is possible to infer how long an annual estimate using the DCPVSIMP model might take on an IBM PC, based on a sample annual simulation using the DCPVDET model on the IBM PC. The DCPVDET sample run took about 7 minutes, so a similar case using the DCPVSIMP model might take about 45 seconds on the IBM PC,

which is probably fast enough to be useful for running multiple cases when optimizing designs.

Lastly, based on performance curves for typical applications as shown in Section 6.3, and based on the statistical validations discussed above, it is concluded that the new simplified method, as implemented in the DCPVSIMP model, can be used with good accuracy in designing and estimating the performance of direct-coupled photovoltaic systems without battery storage.

6.5 Recommendations

Three general areas for continued study and improvements to this work have been identified: Addressing limitations and making enhancements to the DCPVSIMP model; validating direct-coupled system results against measured performance; and investigating whether generalized correlations can be developed to estimate system performance with less computational effort.

The most significant limitation is that the simplified method is not applicable for systems with battery storage. Estimating the condition of a battery and its contribution to serving a system load requires knowing the order of weather and load patterns. The order of days is not preserved by the simplified method. However, a method of re-ordering the sequence of daily clearness indices to approximate long-term average behavior has been proposed by Knight [58] and may be applicable to direct-coupled PV systems. At a minimum, existing battery storage routines could be added to the detailed method (DCPVDET model), and the result would still contribute new modeling capabilities to the

body of available performance models, because there are presently no models available to simulate the long-term performance of any type of direct-coupled load.

Other limitations of the DCPVSIMP model were discussed in Section 5.1.1 and some could be easily remedied; briefly, these include adjusting absorbed radiation to account for varying incidence angles, adding mechanical tracking options, adding southern latitude options, adding economics calculations, and adding more locations, modules, and load types to the existing database. Other effects which have been ignored in developing the new method will be more difficult to address; these include accounting for dirt. shading, long-term degradation, and mismatch on array performance.

The best validation for the DCPVSIMP model would be to compare its estimates to reliable experimental data. The author was unable to obtain such information. As a partial validation, it may be easier to design a controlled experiment testing the short-term performance of various direct-coupled loads.

Subject to the possible improvements and validations discussed above, it may be possible to develop correlations relating the monthly and annual performance of certain direct-coupled loads (e.g., resistive and/or fixed voltage loads) to easily measured variables as shown in Sections 6.3.1 and 6.3.2, thereby eliminating the need for computer modeling to obtain accurate long-term performance estimates.